



Towards an understanding of the controls on $\delta\text{O}_2/\text{N}_2$ variability in ice core records

Romilly Harris Stuart¹, Amaëlle Landais¹, Laurent Arnaud², Christo Buizert³, Emilie Capron², Marie Dumont⁴, Quentin Libois⁵, Robert Mulvaney⁶, Anaïs Orsi^{1,7}, Ghislain Picard², Frédéric Prié¹, Jeffery Severinghaus⁸, Barbara Stenni⁹, and Patricia Martinerie²

¹Laboratoire des Sciences du Climat et de l'Environnement, UMR8212, CNRS – Gif sur Yvette, France

²Université Grenoble Alpes, CNRS, INRAE, IRD, Grenoble INP, IGE, 38000 Grenoble, France

³College of Earth, Ocean, and Atmospheric Sciences, Oregon State University, Corvallis, OR 97331, USA

⁴Univ. Grenoble Alpes, Université de Toulouse, Météo-France, CNRS, CNRM, Centre d'Etudes de la Neige, 38000 Grenoble, France

⁵CNRM, Université de Toulouse, Météo-France, CNRS, Toulouse, France

⁶British Antarctic Survey, Natural Environment Research Council, Madingley Road, Cambridge CB3 0ET, UK

⁷The University of British Columbia, Department of Earth, Ocean and Atmospheric Sciences, Vancouver, Canada

⁸Scripps Institution of Oceanography, University of California, San Diego, La Jolla, CA 92093, USA

⁹Ca' Foscari University of Venice, Department of Environmental Sciences, Informatics and Statistics, Venezia, 30172, Italy

Correspondence: Romilly Harris Stuart (romilly.harris-stuart@lsce.ipsl.fr)

Abstract. Processes controlling pore closure are broadly understood yet defining the physical mechanisms controlling associated elemental fractionation remains ambiguous. Previous studies have shown that the pore closure process leads to a decrease in concentration of small-size molecules (e.g., H_2 , O_2 , Ar, Ne, He) in the trapped bubbles. Ice core $\delta(\text{O}_2/\text{N}_2)$ records – the ratio of O_2 to N_2 molecules in bubbles trapped in ice cores relative to the atmosphere – are therefore depleted owing to this O_2 loss and show a clear link with local summer solstice insolation making it a useful dating tool. In this study, we compile $\delta(\text{O}_2/\text{N}_2)$ records from 14 polar ice cores and show a new link between $\delta(\text{O}_2/\text{N}_2)$ and local surface temperature and/or accumulation rate, in addition to the influence of the summer solstice insolation. We argue that both local climate-driven and insolation forcings are linked to the modulation of snow physical properties near the surface. Using the Crocus snowpack model, we perform sensitivity tests to identify the response of near-surface snow properties to changes in insolation, accumulation rate, and air temperature. These tests support a mechanisms linked to snow grain size, such that the larger the grain size for a given density, the stronger the pore closure fractionation, and hence, lower $\delta(\text{O}_2/\text{N}_2)$ values. Our findings suggest that local accumulation rate and temperature should be considered when interpreting $\delta(\text{O}_2/\text{N}_2)$ as an insolation proxy.

1 Introduction

Ice cores store crucial information for our understanding of past climate variability and atmospheric composition. Interpreting ice core gas records first requires an understanding of the evolution of snow into ice via the firnification processes. Firn is the name given to the layer of unconsolidated snow which makes up the top 50-120m of ice sheets. Atmospheric air moves through porous networks within the firn until a critical depth where vertical diffusion effectively stops, and the pores gradually

become sealed off from the atmosphere to form bubbles trapped within the ice. This depth is called the lock-in depth (LID) and is largely controlled by local accumulation rate, temperature, and possibly the degree of density layering (Schwander et al., 1997; Martinerie et al., 1994; Mitchell et al., 2015).

Measurements of entrapped air can be used to reconstruct past atmospheric compositions, as well as to date the ice cores. One such dating technique, used primarily for deep ice cores from low accumulation sites is orbital dating, which uses insolation curves at a given latitude directly calculated from astronomical variables (Laskar, J. et al., 2004). Records of total air content (Raynaud et al., 2007), $\delta^{18}\text{O}$ of atmospheric O_2 (Extier et al., 2018), and $\delta(\text{O}_2/\text{N}_2)$ (Kawamura et al., 2007; Suwa and Bender, 2008a; Landais et al., 2012; Bouchet et al., 2023) were found to be strongly anti-correlated with insolation curves, and thus, allow for ice core dating using peak matching techniques. The term $\delta(\text{O}_2/\text{N}_2)$ – hereafter, simply $\delta\text{O}_2/\text{N}_2$ – describes the relative difference between the ratio of O_2 to N_2 molecules trapped within the ice and that of the standard atmosphere and is expressed in the delta notation commonly used for stable isotope ratios.

The use of $\delta\text{O}_2/\text{N}_2$ for ice core dating was first proposed by Bender (2002) after observations of an anti-correlation with local summer solstice insolation (hereafter SSI). Data from the Vostok ice core showed that high SSI corresponds to low $\delta\text{O}_2/\text{N}_2$ values and vice versa (Bender et al., 1994). A similar relationship was then observed at numerous other sites such as Dome Fuji (Kawamura et al., 2007) and EPICA Dome C (Landais et al., 2012) in Antarctica, and GISP2 (Suwa and Bender, 2008b) in Greenland. Over orbital timescales, the correlation between $\delta\text{O}_2/\text{N}_2$ and local SSI largely improved when matched on the ice-age timescale rather than the gas-age (Bender, 2002), suggesting that the impact of the insolation on the ice properties occurs at the surface rather than the pore closure depth.

Parallel firn air studies of the open porosity revealed an enrichment in O_2 and other small molecules, such as Ar, Ne and He, compared to air within the closed porosity at the close-off depth (COD), providing further evidence of size-dependent fractionation during pore-closure (Battle et al., 1996; Huber et al., 2006; Severinghaus and Battle, 2006). While the physical mechanisms controlling the amount of fractionation are not fully understood, it is believed that the main processes by which smaller molecules escape during pore closure are; 1) molecular diffusion through the ice lattice, or permeation, resulting from pressure gradients between recently closed pores and neighbouring open pores (Tomoko Ikeda-Fukazawa and Hondoh, 2004; Huber et al., 2006; Severinghaus and Battle, 2006), and 2) diffusion through small openings in the ice matrix, with a threshold of 3.6Å , allowing only molecules with a diameter below 3.6Å to pass through (Huber et al., 2006; Severinghaus and Battle, 2006). Both processes are facilitated by the pore network's capacity to export the fugitive gases back to the atmosphere, which is required for the observed depletion in bulk ice O_2 in bubbles (Fujita et al., 2009).

The simultaneous observations of O_2 depletion in entrapped air bubbles and O_2 enrichment in open porosity, alongside the strong correlation between SSI and $\delta\text{O}_2/\text{N}_2$ on the ice-age scale, led Bender (2002) to develop the hypothesis that the dependence of $\delta\text{O}_2/\text{N}_2$ on local insolation was the result of snow metamorphism near the surface. They, and many subsequent studies, proposed that strong summer insolation drives temperature gradient metamorphism, thus increasing near-surface grain size which propagates through the firn during the firnification process down to the COD (Bender, 2002; Severinghaus and Battle, 2006; Suwa and Bender, 2008a; Fujita et al., 2009; Hutterli et al., 2009). In addition, Fujita et al. (2009) proposed that $\delta\text{O}_2/\text{N}_2$ would be decreased under high SSI conditions due to enhanced density stratification in the deep firn. They argue that



‘summer’ layers – characterised by large grains and relatively low density in the deep firn – close-off deeper and take longer to do so than neighbouring ‘winter’ layers, which are denser and have smaller grains (Picard et al., 2012, 2016). ‘Summer’ layers therefore remain permeable for longer, allowing the O₂ enriched air in open porosity to be exported to the atmosphere, and hence, reducing bulk ice $\delta\text{O}_2/\text{N}_2$ under high SSI conditions (Fujita et al., 2009). While the proposed mechanisms are posited to explain the SSI imprint on $\delta\text{O}_2/\text{N}_2$, they are also influenced by local climate conditions such as temperature, accumulation rate and wind-speed. Indeed, there is a substantial amount of evidence linking local climate conditions with both firn physical properties (McDowell et al., 2020; Casado et al., 2021; Inoue et al., 2023) and deep firn layering (Hörhold et al., 2011).

There is a growing body of evidence for a local climatic imprint on ice core $\delta\text{O}_2/\text{N}_2$ records. Firstly, spectral analysis has revealed climate related 100-ka cyclicity at EPICA Dome C (Bazin et al., 2016) - although such a signal is not apparent at Dome F (Kawamura et al., 2007). Secondly, millennial scale variability in $\delta\text{O}_2/\text{N}_2$ records from GISP2 appeared in-phase with local temperature fluctuations driven by Dansgaard-Oeschger events (Suwa and Bender, 2008b). In parallel, Kobashi et al. (2015) evidenced an anti-phase effect of accumulation rate on $\delta\text{Ar}/\text{N}_2$ records at GISP2 over the last millennia. Like O₂, Ar is a smaller molecule than N₂ so that the same driving mechanisms are invoked for the $\delta\text{Ar}/\text{N}_2$ and $\delta\text{O}_2/\text{N}_2$ variations, but the $\delta\text{Ar}/\text{N}_2$ anomaly tends to be half as large as the $\delta\text{O}_2/\text{N}_2$ anomaly (Bender et al., 1995; Buizert et al., 2023). Kobashi et al. (2015) proposed a direct effect of accumulation rate or temperature on the $\delta\text{Ar}/\text{N}_2$ ($\delta\text{O}_2/\text{N}_2$) variations through the firn depth. The higher the accumulation rate or the lower the temperature, the higher the firn weight and hence the overloading pressures in microbubbles preferentially expelling O₂ and Ar in the LIZ. In contrast, Severinghaus and Battle (2006) proposed that the higher the accumulation rate, the more rapid the burial of bubbles, allowing less time for gases to escape during pore closure.

Using a combination of data and snowpack modelling, we aim to develop our understanding of the formation of the of $\delta\text{O}_2/\text{N}_2$ records, by first, determining the role of local climate parameters, accumulation rate and temperature, on $\delta\text{O}_2/\text{N}_2$ variability, and second identifying potential mechanisms related to snow physical properties using snowpack sensitivity tests. We use a compilation of datasets from 14 ice cores from both Antarctica and Greenland to identify spatial and temporal patterns in $\delta\text{O}_2/\text{N}_2$ depending on local surface conditions. The impacts of SSI and local climate on snow properties are then assessed using the SURFEX-ISBA-Crocus detailed snowpack model (Vionnet et al., 2012). We aim to constrain the influence of near-surface snow properties on $\delta\text{O}_2/\text{N}_2$ variability, potentially contributing to a mechanistic explanation for elemental fractionation during pore closure.

2 Methods

2.1 Ice core sites

We compiled $\delta\text{O}_2/\text{N}_2$ from 18 ice cores from Antarctica and Greenland but use data from 14 of those sites for reasons explained in Section 2.4. Previously published data were measured on ice cores from: Dome Fuji (DF), EPICA Dome C (EDC), Greenland Ice Core Project 2 (GISP2), Law Dome DE08 and DSSW20k, North Greenland Ice core Project (NGRIP), Roosevelt Island Climate Evolution (RICE), Siple Dome (SD), South Pole (SP), Talos Dome (TALDICE), Vostok (VK), and the West Antarctic Ice Sheet Divide (WAISD) ice cores (references for all datasets are presented in Table S2). We also present unpublished data

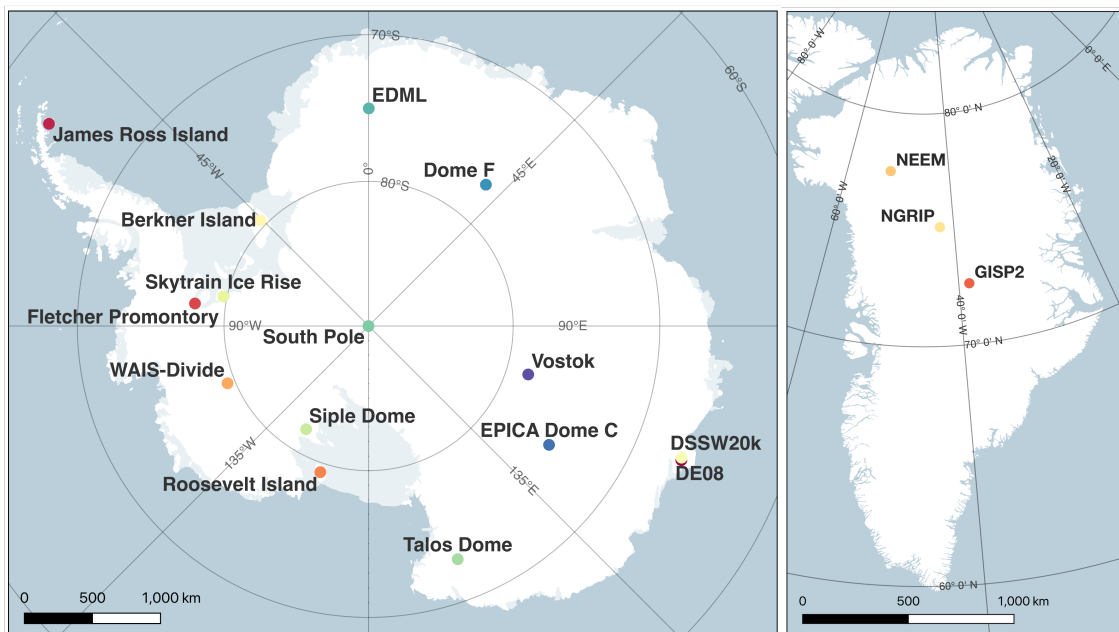


Figure 1. Locations of each ice core site initially included in our study. Maps were made in Quantarctica and QGreenland (Matsuoka et al., 2018; Moon et al., 2023).

from Berkner Island (BI), EPICA Dronning Maud Land (EDML), Fletcher Promontory (FP), GISP2, James Ross Island (JRI), North Greenland Eemian Ice Drilling (NEEM), Skytrain Ice Rise (SIR) and Talos Dome (TALDICE) ice samples (Table S1). Table 1 provides an overview of the site characteristics.

2.2 Analytical techniques for previously unpublished data

- 90 The previously unpublished $\delta\text{O}_2/\text{N}_2$ datasets were measured at the Laboratoire des Sciences du Climat et de l'Environnement (LSCE), with the addition of some GISP2 data measured at Scripps Institution of Oceanography (Scripps). At LSCE, two techniques have been used to extract the trapped air from ice core samples and have been described in previous studies (Landais et al., 2003; Capron et al., 2013; Bazin et al., 2016). In short, the first uses a melt-refreeze technique where ice samples are placed into glass flasks at -20°C while the atmospheric air is evacuated. Samples are then left to slowly melt to release the
- 95 trapped gases, before the samples are refrozen with liquid nitrogen. The extracted air samples are then individually introduced into the line and passed through a CO_2 and water vapour trap, before being trapped in the stainless-steel dip-tube submerged in liquid helium (Landais et al., 2003). The second uses a semi-automated extraction (melt-extraction) line which removes the need for refreezing of the samples (Capron et al., 2010; Bazin et al., 2016). For all datasets measured at LSCE, the average analytical uncertainty for $\delta\text{O}_2/\text{N}_2$ is 0.5‰.
- 100 Unpublished data from the GISP2 core were measured at the Ice Core Noble Gas Laboratory of the Scripps Institution of Oceanography using the melt and refreeze technique (Sowers et al., 1989; Petrenko et al., 2006). Additional information on the



Table 1. Overview of ice core site characteristics. The final three columns show the average annual accumulation rate, the average annual air temperature, and the average surface snow density at each site for present-day conditions.

Site	Latitude (°N)	Longitude (°E)	Elevation (m)	Brittle zone (m)	Accumulation rate (cm w.eq. a ⁻¹)	Temperature (°C)
BI	-79.55	-45.68	890	450-940 ¹	16.2 ¹	-26 ¹
DF	-77.32	39.7	3810	450-1200	2.6 ²	-58 ³
EDC	-75.1	123.35	3233	600-1200	2.8 ⁴	-55 ⁵
EDML	-75	0.04	2892	500-1050	6.4 ⁶	-45 ⁷
FP	-77.9	-82.61	873	- ⁸	38 ⁸	-27 ⁸
GISP2	72.6	-38.5	3200	650-1400	24 ⁹	-31.4 ¹⁰
JRI	-64.2	-57.69	1542	- ⁸	58 ¹¹	-14 ¹¹
LD DE08	-66.72	113.2	1250	525-1200	110 ¹²	-19 ¹²
LD DSSW20k	-66.77	112.81	1370		15 ¹³	-20.7 ¹⁴
NEEM	77.45	-51.6	2450	609-1281	20 ¹⁵	-28.9 ¹⁵
NGRIP	75.1	-42.32	3090	790-1200	17.5 ¹⁶	-31.5 ¹⁶
RICE	-79.36	-161.71	550	650-1300	21 ¹⁷	-23.5 ¹⁸
SD	-81.65	-148.81	621	400-1000	12.4 ¹⁹	-25.4 ²⁰
SIR	-79.74	-78.55	784	- ²¹	13.5 ²²	-26 ²²
SP	-89.99	-98.16	2835	619-1078	8 ²³	-49 ²⁴
TALDICE	-72.82	159.07	2315	667-1002	8 ²⁵	-41 ²⁵
VK	-78.47	106.87	3488	300-720	2.2 ²⁶	-57 ²⁶
WAISD	-79.47	-112.09	1766	650-1300	20.2 ²⁷	-31.1 ²⁷

¹Mulvaney et al., 2007; ²Oyabu et al., 2023; ³Fujita et al., 1998; ⁴Frezzotti et al., 2004; ⁵Stenni et al., 2004; ⁶Oerter et al., 2000; ⁷EPICA community members, 2006; ⁸Mulvaney et al., 2014; ⁹Alley et al., 1993; ¹⁰Alley and Koci, 1988; ¹¹Capron et al., 2013; ¹²Etheridge and Wookey, 1988; ¹³Sturrock et al., 2002; ¹⁴Rubino et al., 2013; ¹⁵Buizert et al., 2012; ¹⁶NGRIP project members, 2004; ¹⁷Winstrup et al., 2019; ¹⁸Bertler et al., 2018; ¹⁹Severinghaus et al., 2001; ²⁰Hamilton, 2002; ²¹Mulvaney et al., 2021; ²²Hoffmann et al., 2022; ²³Lazzara et al., 2012; ²⁴Mosley-Thompson et al., 1999; ²⁵Stenni et al., 2002; ²⁶Arnaud et al., 2000; ²⁷Fegyveresi et al., 2011. All brittle zones are those presented by Neff (2014) unless otherwise stated (and references therein).

GISP2 measurements is available in Martin et al. (2023) where they use the $\delta^{15}\text{N}$ of N_2 from the same samples. An overview of all datasets, both previously published and unpublished, can be found in Table S1 and Table S2, respectively.

2.2.1 New $\delta\text{O}_2/\text{N}_2$ measurements

105 Berkner Island

Measurements were performed on bubbly ice from the Berkner Island ice core every 55 cm (every bag) between 631 m



and 680m, corresponding to 10,269 – 21,350yrBP (Capron et al., 2013). Replicate samples were prepared at LSCE using the melt-refreeze method and measured on a 10-collector Thermo Delta V Plus between March 2010 and March 2011.

110 *EDML*

Nine samples were measured on bubbly ice from the EDML ice core over five depth levels between 328-473 m (327.8 m (4.51 ka BP), 354.2m (4.95 ka BP), 381 m (5.43 ka BP), 467 m (7.04 ka BP), and 473 m (7.16 ka BP)) (Bazin et al., 2013). The samples were prepared using the melt-refreeze method and measured on the 10-collector Thermo Delta V Plus at LSCE. Where possible, the final value of each sample is the average of two replicate measurements at each depth level.

115

Fletcher Promontory

In January 2015, 39 depth levels were measured from the Fletcher Promontory ice core, retrieved in 2012. Measurements were performed approximately every 3 m starting at 289 m down to 388 m. There is currently no published age-scale for the FP ice core. All samples were prepared using the melt extraction method and then measured using a 10-collector Thermo Delta V Plus as LSCE. The final value of each sample is the average of at least two replicate measurements at each depth level.

120

GISP2

New GISP2 $\delta\text{O}_2/\text{N}_2$ data were analysed at Scripps Institution of Oceanography from 643 depths between 1740 and 2400 m (13 to 50 ka BP), with the $\delta^{15}\text{N}$ data from these analyses reported previously (Martin et al., 2023). Most of the samples were analysed in replicate. Measurements were performed in several campaigns between 2017-2020 and referenced to La Jolla pier air. Measurements were performed using a melt-refreeze method (Petrenko et al., 2006).

125

James Ross Island

Between February and March 2011, measurements were performed at 16 depth levels on the James Ross Island Ice core. The depth resolution varied between 2-50 m starting at 52 m until 363 m. Samples were prepared using the melt extraction method and then measured using a 10-collector Thermo Delta V Plus as LSCE. The final value of each sample is the average of at least two replicate measurements at each depth level.

130

NEEM

Clathrate ice from the NEEM ice core was measured between February and April 2011, a year after the core was retrieved. A total of 119 depth levels were sampled were measured at varying resolutions over the following intervals: 55cm intervals (every bag) between 1757-1773 m (38.127 – 39.735 ka B2k), 5.5 m intervals (every 10 bags) between 2205 and 2370 m (108.56 - 120.237 ka B2k), every 2 bags from 2375-2434 m (no published age-scale available below these depths), and 5.5 m intervals (every 10 bags) between 2436 and 2519 m (Gkinis et al., 2021; Rasmussen et al., 2013). In total, samples from 119 depth levels were prepared using the melt-refreeze method and measured using a 10-collector

135



140 Thermo Delta V Plus as LSCE. The final value of each sample is the average of at least two replicate measurements at each depth level.

Skytrain Ice Rise

145 Measurements were performed on bubbly ice from the Skytrain Ice Rise ice core between March and April 2021. Samples were taken sporadically (1-15m intervals) at 16 depth levels between 307 and 436 m depth (4.707-11.696 ka BP) (Mulvaney et al., 2023). Each sample was prepared at LSCE using the melt extraction method and subsequently measured on a 10-collector Thermo Delta V Plus. The final value of each sample is the average of at least two replicate measurements at each of the 16 depth levels.

TALDICE

150 Numerous measurements have been done on bubbly and clathrate ice from TALDICE between 2008 and 2022 at LSCE. A total of 308 depth levels were measured at varying intervals starting at 155 m down to 1617 m. Published age-scales reach 1548 m, giving an age range of 1.55-343 ka for TALDICE samples (Buiron et al., 2011; Crotti et al., 2021). All samples were prepared using the melt extraction technique and measured on the 10-collector Thermo Delta V Plus. Some measurements between 1356-1620 m depth have been published previously and are available in Crotti et al. (2021).

2.2.2 Corrections

155 Chemical and pressure imbalance corrections are applied to the measurements during data processing (Landais et al., 2003). In addition, all data are corrected for gravitational fractionation in the firn using $\delta^{15}\text{N}$ of N_2 from the same samples.

$$\delta O_2/N_2 \text{ grav} = \delta O_2/N_2 - 4 \cdot \delta^{15}N \quad (1)$$

160 Gas loss effects during coring and ice core storage are well documented to modify $\delta O_2/N_2$, causing significant depletion in O_2 in clathrate ice stored above -50°C (Ikeda-Fukazawa et al., 2005; Kawamura et al., 2007; Landais et al., 2012). Ikeda-Fukazawa et al. (2005) proposed an equation to correct for gas loss effects during storage at different temperatures. However, given the incomplete storage history for all ice cores we do not attempt to correct for storage gas loss, but rather define rejection criteria outlined in Section 2.2.3.

2.2.3 Data rejection criteria

165 At the transition zone between bubbly ice and clathrate ice (hereafter the brittle zone) strong elemental fractionation occurs whereby the air in the gas phase has a very different composition to that in the clathrate hydrates, thus making the interpretation of gas measurements unreliable at these depths (Bender, 2002). Measurements from brittle ice tend to be characterised as having increased mean $\delta O_2/N_2$ (usually in excess of 0‰) and strong data scattering, expressed as a high standard deviation. All measurements from Berkner Island fall within the reported brittle zone but show no scattering, and are therefore included in our analysis. This is also observed at other sites – where some depths defined as the brittle zone show no evidence of scattering – and is expected to be due to the approximation of the brittle zone depths. To avoid adding biases to our analysis, measurements



170 from brittle ice from all other sites are removed, leaving the measurements from bubbly ice above, and the clathrate ice below the brittle zone. Additional scattering in elemental ratios, characterised by a standard deviation of 6.2‰ compared to 1.8‰ in non-brittle ice, is observed below the brittle zone in the WAIS-Divide record between 1300-1500m (Shackleton, 2019). Similar effects were observed on the EDC and TALDICE ice cores (Lüthi et al., 2010) and the Dome Fuji ice core (Oyabu et al., 2021). Data influenced by this scattering effect was also removed from our analysis.

175 The different storage histories of ice used for each measurement campaign need to be considered before interpreting the data to account for gas loss effects (Section 2.2.2). Successive $\delta\text{O}_2/\text{N}_2$ measurements from TALDICE and GISP2 clathrate ice samples show strong depletion of O_2 through time (Supplement S1), which is consistent with observations from Dome C (Bouchet et al., 2023). Having separated the datasets into bubbly ice and clathrate ice – by taking the data above and below the brittle zone – we systematically reject measurements from clathrate ice stored at -20°C for over 3 years, or at -36°C for more
180 than 4 years. Bubbly ice stored at these same temperatures appear largely unaffected by gas loss (Supplement S1), with the exception of Vostok (Suwa and Bender, 2008a). Applying these criteria to the datasets results in the removal of all data from NGRIP and Vostok, as well as sections of data from other sites. The remaining 14 datasets are presented in Table 3 and were used to analyse the drivers of $\delta\text{O}_2/\text{N}_2$ variability.

2.3 Modelling near-surface snow properties

185 The second component of our study addresses the modelled response of snow physical properties to perturbations in SSI, accumulation rate, and temperature with the aim of identifying which properties may be influencing elemental fractionation during pore closure. We use the SURFEX-ISBA-Crocus detailed snowpack model (Crocus hereafter) to simulate snowpack evolution (Vionnet et al., 2012). Crocus simulates changes in snow physical properties induced by surface metamorphism and the evolution of these properties with depth. The model is forced by ERA5 reanalysis data (Hersbach et al., 2020), and
190 the snowpack is initialised with measurements of snow density, effective optical radius of snow grains and snow temperature. Optical radius is defined as the radius which snow grains would have for their surface area-to-volume ratio if they were spherical (Domine et al., 2006). Optical radius is thus directly linked to specific surface area (SSA), defined as the surface area of snow at the ice-air interface per unit mass (units m^2kg^{-1}) (Legagneux et al., 2002), via the following equation:

$$\text{SSA} = \frac{3}{r_{opt} \cdot \rho_{ice}} \quad (2)$$

195 Where r_{opt} is the optical radius and ρ_{ice} is the density of ice (Gallet et al., 2014). We use this model to assess changes in snow physical properties near the surface which are invoked to explain $\delta\text{O}_2/\text{N}_2$ variability. Dome C is used as the test site given the abundance of snowpack observations as well as high resolution $\delta\text{O}_2/\text{N}_2$ data.

2.3.1 Crocus model description

Crocus is a 1-dimensional model which simulates the evolution of snow properties with time and depth on a layer-by-layer
200 basis, i.e., in a Lagrangian framework (Vionnet et al., 2012). A detailed description of the model can be found in Vionnet et al. (2012). Briefly, the initial number of layers is defined by the user, with the thickness of each layer allowed to change along



the simulation (layer thickness ranging from millimetres to metres thick). The maximum number of layers available in the model was increased from 50 to 80 to account for the higher number of thin layers forming at Dome C than at Alpine sites. Once the simulated snowpack consists of 80 layers, the aggregation scheme merges internal neighbouring layers with similar properties allowing a new surface layer to form. The key physical processes incorporated into Crocus for dry snow conditions are accumulation of snowfall, snow metamorphism, compaction of snow by the wind, compaction due to the weight of the overlying layers, absorption of solar radiation, heat diffusion, and surface energy budget.

For our study, two fundamental user-defined model components are the snow metamorphism and radiative transfer schemes. We use the semi-empirical model from Flanner and Zender (2006) (F06) for the metamorphism scheme which describes the evolution of optical radius with time. F06 was found to be the most appropriate formulation for Dome C conditions (Carmagnola et al., 2014; Libois et al., 2014). To successfully reproduce the snow temperature profile – vital for realistically simulating snow metamorphism – the Two-streAm Radiative TransfER in Snow model (TARTES) is used to account for vertical distribution of absorbed solar radiation in the snowpack (Libois et al., 2013). TARTES also considers the effect of impurities on snow temperature via albedo. For Dome C, we include black carbon content which is set to 3 ng g^{-1} (Warren et al., 2006; Libois et al., 2015). In this study, we assess the simulated snow density, snow temperature and snow SSA from Crocus model outputs.

2.3.2 Dome C specific Crocus configuration

Crocus was initially developed for alpine or sub-polar regions with seasonal snowpacks. Libois et al. (2014) modified multiple components of the Crocus model to improve its suitability to high latitude sites with low accumulation rates - specifically for Dome C. The modifications are extensively described in Libois et al. (2014) and were implemented into the current version of Crocus for this study. The changes are as follows:

1. *Fresh snow properties*: The parameterisation of fresh snow density is based on temperature and wind-speed which results in an unrealistically low density for Dome C conditions (50 kg m^{-3}). Fresh snow density is fixed to a minimum of 170 kg m^{-3} - the lowest fifth percentile from Dome C observations (Libois et al., 2014). Similarly, fresh snow SSA is set to $100 \text{ m}^2 \text{ kg}^{-1}$ instead of $65 \text{ m}^2 \text{ kg}^{-1}$ used in the standard version of the model (Grenfell et al., 1994; Libois et al., 2014).
2. *Wind-induced compaction*: At low-accumulation sites, the snow can remain at the surface for prolonged periods of time. The long exposure time to surface winds facilitates compaction, and hence increases density. The maximum surface snow density is increased from 350 kg m^{-3} to 450 kg m^{-3} to account for this effect (Albert et al., 2004; Libois et al., 2014).
3. *Aggregation scheme*: The formation of a new snow layer requires a minimum amount of snowfall. Due to the low accumulation rate at Dome C, the amount of snowfall needed to form a new layer was decreased from 0.03 mm h^{-1} to 0.003 mm h^{-1} . In the instance when the snowpack has the maximum number of layers (80) at the time a new snow layer is formed, layers with similar properties will be aggregated, resulting in a smoothed signal. The aggregation scheme



235 was disabled for the top 6 layers to resolve realistic near-surface snow temperature profiles and gradients, required to accurately simulate snow metamorphism.

2.3.3 Model initialisation

The snowpack was initialised with density and optical radius profiles measured in January 2010 at Dome C down to 20m (Champollion et al., 2019), and snow temperature data from a probe installed at Dome C in 2012 with 5 cm resolution near the surface, coarsening with depth down to 12 m. ERA5 reanalysis data from Dome C was used to force the model at 3-hourly resolution over the period between 1st January 2000 and 1st December 2020 (Hersbach et al., 2020). The model requires atmospheric forcings for air temperature, accumulation rate, wind speed and direction, incoming shortwave and longwave radiation, and specific humidity. ERA5 gives a mean annual snowfall rate between 2000 and 2020 of 2.3 cm w.eq. a⁻¹, and as such, the snowfall rate was multiplied by 1.2 to match the observed mean annual accumulation rate of around 2.8 cm w.eq. a⁻¹ (Frezzotti et al., 2004; Libois et al., 2014). To ensure that at least the top 1m consists of accumulated snow, a 100-year spin up was used by running the forcing file 10 times between 2000 and 2010, followed by the period from 2000 to 2020. The outputs from 2010 to 2020 were then used for analysis.

2.3.4 Sensitivity tests

The sensitivity of snowpack properties to perturbations in surface forcings are tested by modifying one of three forcing parameters: incoming shortwave radiation, accumulation rate, or 2 m air temperature. The magnitude of the perturbation to each parameter correspond to minimum and maximum values reconstructed over the last 800 ka. We use shortwave radiation as a proxy of insolation and scale the values in proportion to the SSI values. A total of seven simulations are used to perform sensitivity analysis and are outlined in Table 2. The model configuration and initial snow profile were kept constant for each simulation; only the tested parameter in the atmospheric forcing file was modified as follows:

Table 2. Overview of modifications made to forcing test parameter in Crocus snowpack sensitivity test scenarios.

Simulation	Reference	SSI min	SSI max	A min	A max	T min	T max
Incoming SWR (Scaled)	100%	85%	111%	100%	100%	100%	100%
Accumulation rate (cm w.eq. a ⁻¹)	2.8	2.8	2.8	1.0	4.1	2.8	2.8
Air temperature (°C)	-55	-55	-55	-55	-55	-65	-51

255 *Summer solstice insolation (SSI)*: Over the last 1000 years, the average SSI at 75.1°S was 544 W m⁻² (Laskar, J. et al., 2004), compared to 462 W m⁻² and 601 W m⁻², corresponding to minimum and maximum SSI over the past 800 ka. To translate to forcing perturbations, the incoming shortwave radiation (SWR) is scaled by 85% and 111%, respectively to reach the target values (462 W m⁻² and 601 W m⁻²). No additional modifications are applied to annual distribution of SWR.

Annual mean accumulation rate (A): Present-day accumulation rate at Dome C is set to 2.8 cm w.eq. a⁻¹ in the ERA5 forcing. Hereafter, accumulation rate is expressed as ice equivalent centimetres per year. ERA5 snowfall was scaled by 36%



to reach the target accumulation rate of $1.0 \text{ cm w.eq. a}^{-1}$, representing the 800ka minimum, and 146% to produce an accumulation rate of $4.1 \text{ cm w.eq. a}^{-1}$ which corresponds to the 800ka maximum (Bazin et al., 2013).

265 *Annual mean air temperature (T)*: Snowpack sensitivity to air temperature is tested by decreasing the 2m air temperature by 10°C for glacial conditions (Jouzel et al., 2007), and applying a 4°C , increase to represent 800ka maximum temperatures. We note, however, that borehole temperature measurements and delta-age are more consistent with a 5°C cooling (Buizert, 2021). Furthermore, these temperature modifications do not include changes in seasonal temperature variability but suffices for the purpose of identifying bulk changes in the snow properties. The average seasonal cycle is kept constant with an average amplitude of 35°C .

270 It is important to highlight that at polar sites accumulation rate is dependent on temperature, and temperature is influenced by insolation, such that these parameters are not independent. However, we use the model to constrain the influences of each forcing parameter in an independent manner to understand the mechanisms, even if, in reality, these parameters are interdependent.

3 Results

3.1 Influence of SSI and local climate on $\delta\text{O}_2/\text{N}_2$ variability in ice cores

275 Figure 2 shows $\delta\text{O}_2/\text{N}_2$ versus SSI for EDC, Dome F and South Pole. These three sites are used owing to their long temporal range and high-resolution $\delta\text{O}_2/\text{N}_2$ measurements, but with negligible gas loss. The regression slopes vary between $-0.09 \pm 0.006 \text{‰.m}^2.\text{W}^{-1}$ for South Pole to $-0.06 \pm 0.005 \text{‰.m}^2.\text{W}^{-1}$ for EDC. The regression for Dome F falls within 2 standard deviations (2σ) of the regression for EDC, but the regression for South Pole falls just outside the 2σ uncertainty. Furthermore, the $\delta\text{O}_2/\text{N}_2$ is shifted for South Pole compared to EDC, evidenced by the increased y-intercept from 18.9‰ at 280 EDC to 40.6‰ at South Pole. Inter-site differences in the dependence of absolute $\delta\text{O}_2/\text{N}_2$ on SSI suggest additional factors are influencing the records, such as accumulation rate – which at South Pole is over double that of both EDC and Dome F – or integrated summer insolation. In the following sections, we provide evidence for the influences of accumulation rate and air temperature on $\delta\text{O}_2/\text{N}_2$, in addition to SSI, using both spatial (inter-site) and temporal (EDC ice core) variability of $\delta\text{O}_2/\text{N}_2$.

3.1.1 Inter-site comparison of mean $\delta\text{O}_2/\text{N}_2$

285 In addition to the $\delta\text{O}_2/\text{N}_2$ datasets, we compile accumulation rate and temperature reconstructions from each site covering the same depth range as the $\delta\text{O}_2/\text{N}_2$ data. Due to the inclusion of measurements from varying depths, and thus, ages, between sites, we include the range of accumulation rates and temperatures to indicate the climate histories for each site (Table 3). The data are presented in Figure 3 for a) 1000 year averaged SSI, b) accumulation rate, and c) temperature. Error bars in panel a) and b) indicate the range of values with the exceptions of; Berkner Island and James Ross Island, where the minimum, maximum, 290 and mean accumulation rate and temperature values are approximated as last glacial maximum values (Capron et al., 2013), the present day values, and the mean of these two values, respectively; and, Law Dome sites DE08 and DSSW20k, where

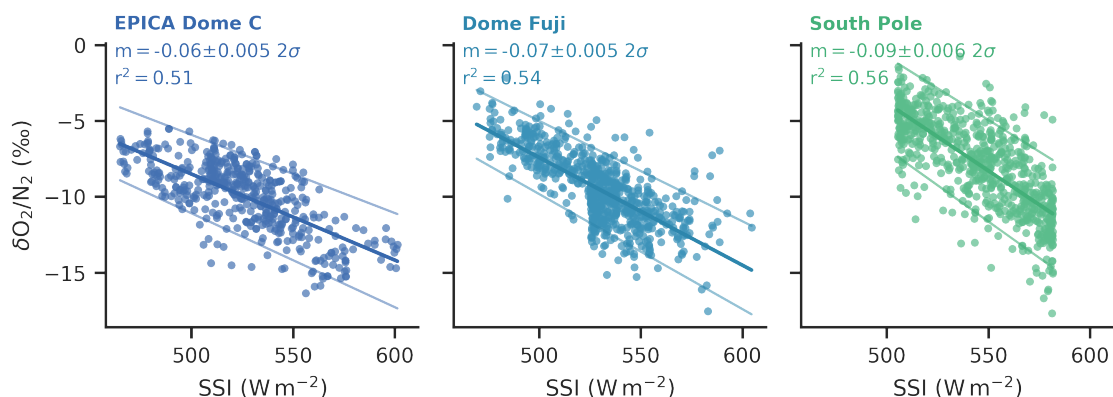


Figure 2. Scatter plots showing the negative correlation between SSI and $\delta O_2/N_2$. Significant negative correlations (over 99% confidence) are observed using high resolution data from Dome C (dark-blue; Bouchet et al., 2023), Dome F (mid-blue; Kawamura et al., 2007; Oyabu et al., 2021), and South Pole (green; Severinghaus et al., 2019). The slope (m , units $\% \cdot m^2 \cdot W^{-1}$) and r^2 values are presented for each site.

only the present-day values are used. We acknowledge that the former approximation may introduce a bias towards cold, low-accumulation conditions.

As expected, mean $\delta O_2/N_2$ is anti-correlated with SSI ($r = -0.47$, $p < 0.1$) with a slope of -0.07 , the same as observed in Figure 2. However, in addition to the influence of SSI, we find a stronger, more significant correlation between mean $\delta O_2/N_2$ and both temperature ($r = 0.72$, $p < 0.001$) and the natural log of accumulation rate ($r = 0.81$, $p < 0.001$) – the logarithmic dependence suggesting increased sensitivity at low accumulation rates. The linear model in Figure 2b indicates that a doubling of accumulation rate would result in a 1.5‰ increase in $\delta O_2/N_2$ ($\delta O_2/N_2 = 2.2 \cdot \log(A) - 12$). However, it is important to note that temperature and the logarithm of accumulation rate are strongly correlated in Antarctica, such that the correlations seen in panels (a) and (b) of Figure 3 are dependent on one another.

Large residuals in Figure 2a can partially be attributed to the use of 1000-year average SSI instead of averages over the same time periods as the $\delta O_2/N_2$ data. This would require age-scales for all sites. Deviations from the $\delta O_2/N_2$ -SSI regression line may also be attributed to discrepancies in site latitude resulting from the ice flow speed at different sites. Indeed, data from NEEM were measured on ice between 1757 and 2525 m depth (approximately 38-130 ka), when the ice would have been upstream of the current site at a lower latitude (Rasmussen et al., 2013; Members, 2013). Berkner Island, NEEM and Siple Dome fall below the regression lines in panels b) and c). For Berkner Island, this may be linked to the method used to determine the mean accumulation rate and temperature values. Other explanations may be linked to procedural artefacts such as gas loss during storage.

3.1.2 Temporal variability of $\delta O_2/N_2$ at Dome C

High resolution data is required to investigate the temporal variability in $\delta O_2/N_2$ as a function of accumulation rate, temperature, and SSI. The δ -deuterium (δD) record from water isotope measurements is used as a qualitative proxy for accumulation

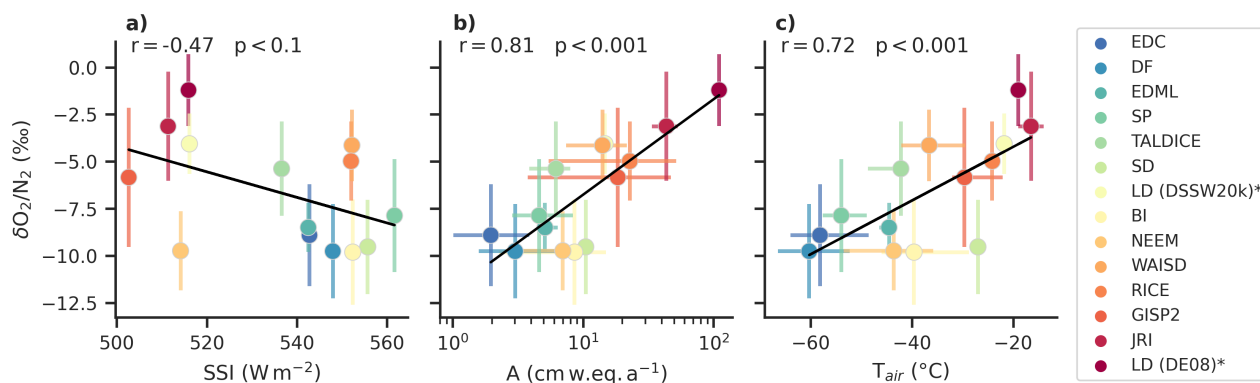


Figure 3. Scatterplots showing the dependence of $\delta\text{O}_2/\text{N}_2$ on the a) SSI, b) accumulation rate (A), and c) annual average temperature (T_{air}). Each point represents the mean values for each site over the depth interval of included $\delta\text{O}_2/\text{N}_2$ data for each site (Table 3). Error bars represent the range of values over the depth interval. Error bars on y-axis show the standard deviation of $\delta\text{O}_2/\text{N}_2$ measurements, and the x-axis in b) and c) show the range in accumulation rate and temperature. In each panel, the black line shows the linear regression between $\delta\text{O}_2/\text{N}_2$ and each parameter, along with the associated correlation coefficient (r) and p-value. Data shown here are presented in Table 3, while information on the individual datasets can be found in Table S1 and S2 in the supplement. *Present-day accumulation rate and temperature have been used or the two Law Dome sites; DE08 and DSSW20k.

rate and temperature, whereby higher δD values are generally associated with increased accumulation rate and temperature in ice cores from the East Antarctic plateau (Jouzel et al., 2007; Parrenin et al., 2007). The following analysis uses high resolution $\delta\text{O}_2/\text{N}_2$ and δD measurements from the EPICA Dome C (EDC) ice core (Jouzel et al., 2007; Bouchet et al., 2023),
 315 both on the AICC2012 ice-age scale (Bazin et al., 2013). $\delta\text{O}_2/\text{N}_2$ records used for orbital dating require the filtering of noise and millennial-scale variability (Kawamura et al., 2007; Landais et al., 2012). However, no filtering is applied here in order to resolve variability over shorter timescales. The new measurements cover five distinct sections of the core between 111 and 539 ka BP (Bouchet et al., 2023). We primarily focus on the longest section between 180-259 ka BP (1980-2350 m) which covers MIS 7.

320 In Figure 4, the $\delta\text{O}_2/\text{N}_2$ curve is dominated by the SSI cyclicity, as has been documented previously (e.g., Landais et al., 2012). Superimposed onto this signal are millennial-scale peaks in $\delta\text{O}_2/\text{N}_2$ which appear to coincide with peaks in δD , highlighted by grey bars in Figure 4c. To evaluate additional climatic signals in the EDC $\delta\text{O}_2/\text{N}_2$ records, we first remove the SSI signal from the record using the residuals of the linear regression between $\delta\text{O}_2/\text{N}_2$ and SSI (Figure 2b). We observe that, in addition to the millennial-scale variability, some long-term variability remains which would not be expected if $\delta\text{O}_2/\text{N}_2$ was
 325 controlled by SSI alone. Indeed, there is a stronger significant positive correlation between δD and SSI- $\delta\text{O}_2/\text{N}_2$ residuals on the ice-age scale between 190-260 ka BP (Figure 4d; $r=0.68$, $p<0.001$), than δD and $\delta\text{O}_2/\text{N}_2$ (Figure 4e; $r=0.43$, $p<0.001$). This suggests a positive correlation with accumulation rate and temperature and shares analogy with the spatial positive correlation between $\delta\text{O}_2/\text{N}_2$ and both accumulation rate and temperature (Figure 3). Applying the same analysis to the other periods of



Table 3. Information on $\delta\text{O}_2/\text{N}_2$ datasets from each site after removing measurements influenced by gas loss. Presented are; the $\delta\text{O}_2/\text{N}_2$ mean (μ), standard deviation (σ), and number of $\delta\text{O}_2/\text{N}_2$ measurements depths (N); the depth range of $\delta\text{O}_2/\text{N}_2$ measurements; the mean (μ), minimum (min) and maximum (max) accumulation rate (A), and the mean (μ), minimum (min) and maximum (max) temperature (T) over the same depth range as the $\delta\text{O}_2/\text{N}_2$ data; and site latitude. The depth ranges have been rounded.

Site	$\delta\text{O}_2/\text{N}_2$ (‰)			Depth (m)	A (cm w.eq. a ⁻¹)			T (°C)			Lat (°N)
	μ	σ	N		μ	min	max	μ	min	max	
*BI ¹	-9.81	2.8	64	609-694	8.6	2.3	14.9	-39.6	-46.0	-28.7	-79.6
DF ²	-9.76	2.5	913	113-449, 1410-2500	3.0	1.6	7.2	-60.3	-66.5	-52.3	-77.3
EDC ³	-8.91	2.7	823	1421-3189	2.0	1.0	3.9	-58.2	-64.0	-48.5	-75.1
EDML ⁴	-8.5	1.3	5	596-860	5.1	5.1	6.4	-44.5	-46.5	-43.7	-75.0
GISP2 ⁵	-5.84	3.7	182	73-648, 1515-2428	18.4	3.8	47.0	-29.6	-32.1	-22.1	72.58
*JRI ⁶	-3.13	2.9	16	52-364	43.5	33.8	53.3	-16.5	-19.0	-14.0	-64.2
**DE08 ⁷	-1.21	1.9	8	175-218	110	-	-	-19.0	-	-	-66.72
**DSSW20k ⁸	-4.06	1.6	4	61-63	14.7	-	-	-21.8	-	-	-66.77
NEEM ⁹	-9.74	2.1	119	1757-2525	7.0	2.6	10.5	-43.6	-53.5	-35.8	77.42
RICE ¹⁰	-4.98	2.1	387	60-344	22.8	5.4	51.6	-24.3	-	-	-79.36
SD ¹¹	-9.53	2.5	68	69-400	10.5	9.9	11.0	-27.0	-28.2	-26.1	-81.65
SP ¹²	-7.87	3	691	125-617, 1078-1751	4.6	2.9	98.3	-54.0	-57.7	-48.9	-89.99
TALDICE ¹³	-5.38	2.5	68	155-669, 1003-1402	6.2	3.9	8.0	-42.2	-48.7	-41.1	-72.82
WAISD ¹⁴	-4.14	1.9	433	80-648, 1602-3397	14.1	7.4	21.7	-36.6	-42.1	-29.5	-79.47

References for $\delta\text{O}_2/\text{N}_2$ data, accumulation rate, and temperature correspond to a, b, and c, respectively. ¹This study^a, Capron et al., 2013^{b,c}; ²Kawamura et al., 2007^a, Oyabu et al., 2021^a, Watanabe et al., 1999^b, Uemura et al., 2018^c; ³Bouchet et al., 2023^a, Extier et al., 2018^a, Bazin et al., 2013^b, Jouzel et al., 2007^c; ⁴This study^a, Bazin et al., 2013^b, Stenni et al., 2010^c; ⁵This study^a, Suwa and Bender, 2008b^a, Cuffey and Clow, 1999^b, Clow, 1999^c; ⁶This study^a, Capron et al., 2013^{b,c}; ⁷Buizert et al., 2020^a; Rubino et al., 2013^b, Etheridge and Wookey, 1988^c; ⁸Buizert et al., 2020^a, Rubino et al., 2013^b, Morgan et al., 1997^c; ⁹This study^a, Rasmussen et al. (2013)^{b,c}; ¹⁰Lee et al., 2020^a, Winstrup et al., 2019^b, Bertler et al., 2017^c; ¹¹Severinghaus, 2009^a, Buizert, 2021^{b,c}; ¹²Severinghaus, 2019^a, Kahle et al., 2020^{b,c}; ¹³This study^a, Bazin et al., 2013^{b,c}; ¹⁴Severinghaus, 2015^a, Fudge et al., 2017^b, White et al., 2019^c.

*JRI and BI using LGM and present day values (Capron et al., 2013) as the maximum and minimum.

** Present-day A and T are used for both Law Dome sites.

high-resolution measurements results in significant positive correlations for all but the period between 409 and 449 ka BP (Figure S3 in Supplement).

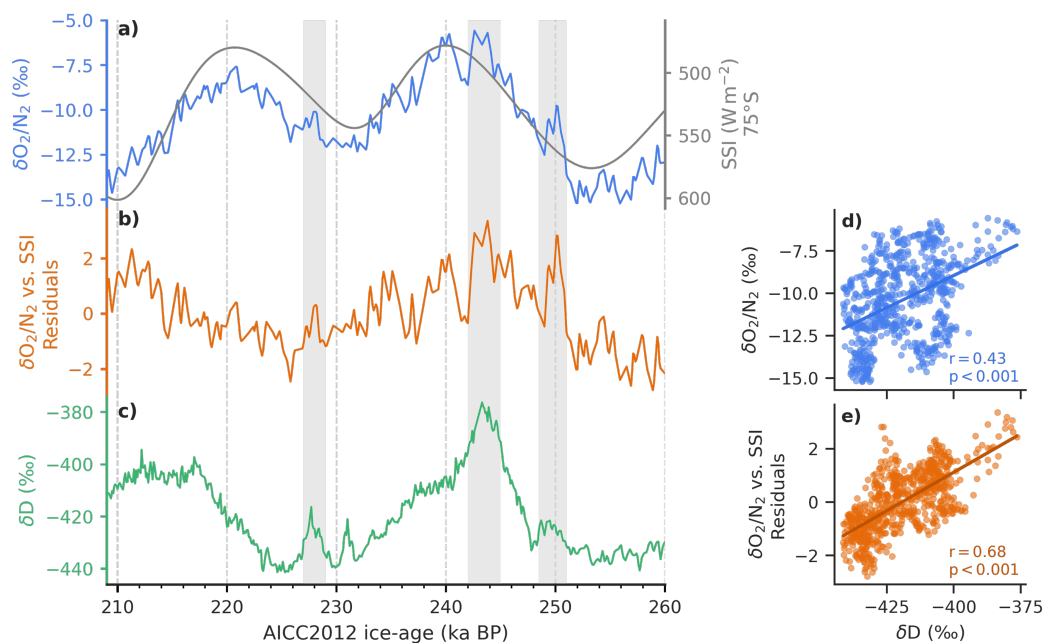


Figure 4. Evolution of $\delta\text{O}_2/\text{N}_2$, SSI and δD on the AICC2012 ice age timescale from Dome C (Bazin et al., 2016; Bouchet et al., 2023). Panel a) presents the $\delta\text{O}_2/\text{N}_2$ (blue) with SSI on the right y-axis (grey), b) the $\delta\text{O}_2/\text{N}_2$ -SSI residuals (orange), and c) δD (green), over the period between 210 and 260 ka BP. Correlations between δD and $\delta\text{O}_2/\text{N}_2$, and between δD and the $\delta\text{O}_2/\text{N}_2$ -SSI residuals are presented in d) and e), respectively.

3.2 Crocus model results

3.2.1 Crocus model evaluation for Dome C

The Crocus model outputs are first evaluated by comparing the reference simulation (Ref in Table 2) to observational data from Dome C. Simulated density and SSA profiles are compared to data from Libois et al. (2014), measured daily between
 335 23^{rd} November 2012 and 16^{th} January 2013 at two sites within 600m of Concordia station, Dome C. Density was measured at 2.5cm resolution down to 25cm, while SSA was measured at 1cm depth intervals down to 50cm. Snow temperature at Dome C has been continuously measured since 2012 at 30-minute intervals. Simulated snow density and SSA were interpolated to a fixed grid of 1cm depth resolution and a 24-hour timestep between 2010-01-01 and 2020-12-01, while snow temperature was interpolated onto a 1mm by 6-hourly grid over the same time period.

340 Density and SSA outputs presented in Figure 5a and b are averaged values over the measurement period (23^{rd} November 2012 and 16^{th} January 2013). For the most part, the observations fall within the range of the simulations. The simulated SSA profile is consistently within one standard deviation of the measurements below 10cm, above this depth, simulated SSA is overestimated by up to $10\text{m}^2\text{kg}^{-1}$. In contrast, density is well-simulated throughout the top 25cm. Small standard deviations



associated with simulated density and SSA, suggests that variability is not well reproduced. As discussed in Libois et al. (2014),
345 the standard version of Crocus is unable to reproduce density and SSA variability with depth due to its one-dimensional nature.
For the purpose of our study, we consider the standard version sufficient to assess the overall sensitivity of snowpack properties
to perturbations in forcings.

Snow temperature in Figure 5c covers the period between 23rd November 2019 and 16th January 2020. A 3°C cold bias
is apparent, but the mean falls within 1 σ of the observations. Figure 5d presents distributions of the stacked January snow
350 temperatures between 2016 and 2020, further showing this 3°C cold bias during summer ($-37.1 \pm 3.6^\circ\text{C}$ and $-34.4 \pm 4.1^\circ\text{C}$ for
Crocus outputs and observations, respectively). However, stacked July snow temperatures are well simulated with a 1 m mean
of $-64.7 \pm 4.5^\circ\text{C}$ and $-63.9 \pm 5^\circ\text{C}$ from Crocus outputs and observations, respectively. The overestimation of SSA in the top
10 cm may be linked to the summer cold bias in near-surface snow temperature, reducing the rate of snow metamorphism in
near-surface grains.

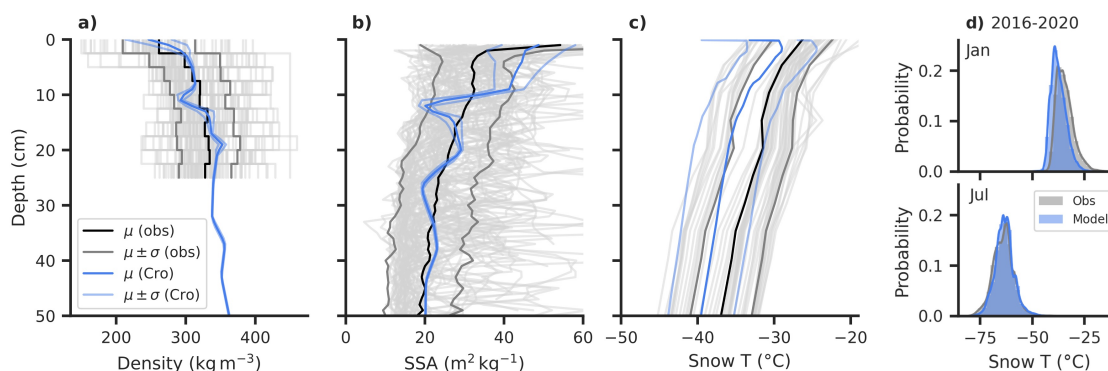


Figure 5. Comparison of observations and Crocus simulated snowpack profiles. SSA (a) and density (b) profiles represent the average from 23rd November 2012 and 16th January 2013, to cover the measurement period (Libois et al., 2014). The snow temperature (c) profiles both from Crocus and the observations are the average from 23rd November 2019 and 16th January 2020. Faded grey lines represent individual profiles from observations, and the shaded bands show the standard deviations. Snow temperature distributions (d) from January and July between 2016 and 2020.

355 3.2.2 Simulated response of snowpack properties to surface perturbations

Sensitivity tests were run using the Crocus model to assess the response of near-surface snowpack properties to perturbations in local surface forcings. The following analysis uses optical radius as a measure of grain size – which is directly linked to SSA and the density of ice (Section 2.3.1) – and focuses on the response of near-surface snow density and grain size to the six scenarios outlined in Table 2. We firstly assess the bulk changes in physical properties before looking at the variability with
360 depth.

3.2.3 Bulk snowpack sensitivity

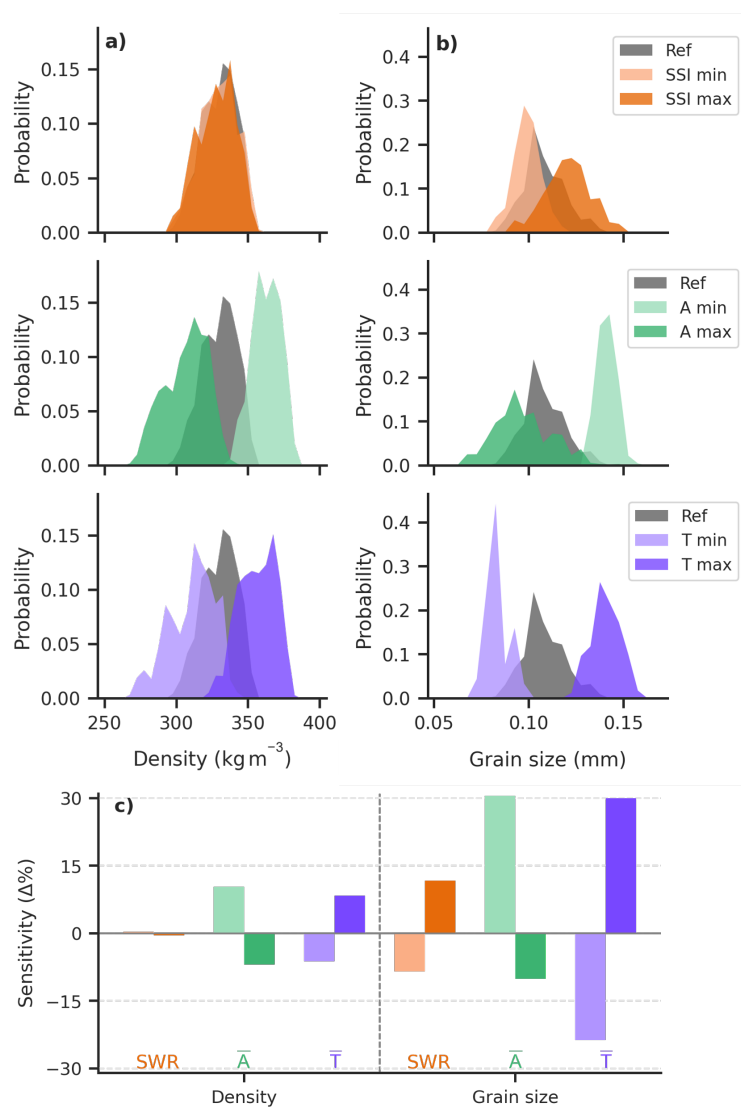


Figure 6. Comparison of density and grain size (r_{opt}) over the top 20cm from Crocus sensitivity simulations. Distributions of a) density and b) grain size outputs from each test simulation are compared the reference simulation (bin size is 5 kg m^{-3} , and 0.005 mm). In panel c) bars represent the percentage change in mean density and mean grain size for perturbations in SSI (orange), accumulation rate (green), and temperature (purple); with the decreased scenarios represented by the faded colour, and the increased by the bold colour.

Numerous studies have suggested that modifications in near-surface density and grain size are key parameters influencing elemental fractionation during pore closure (e.g., Bender, 2002; Fujita et al., 2009). Figure 6c and 6d show the mean difference in density and grain size from the Dome C reference simulation (Ref) and each of the test scenarios (outlined in Table 2).



365 Overall, grain size is more sensitive to changes in surface forcing than density in the upper 20 cm. The sensitivity tests reveal that a 15% decrease in SSI (SSI min) decreases grain size by 8% and an 11% increase in SSI (SSI max) causes a 12% increase in grain size. Both directions of perturbation result in <1% change in density. The magnitudes of change in both density and grain size are much larger under accumulation rate and temperature perturbations than under SSI perturbations.

Accumulation rate and temperature have the opposite effect on density and grain size. A 4°C increase in temperature (T max) increases density and grain size by 8% and 29%, respectively, while an increasing the accumulation rate to 4.1 cm w.eq. a⁻¹ (A max) results in a 7% decrease in density and a 10% decrease in grain size. These opposing influences of accumulation rate and temperature on snow properties at first appears to contradict the observations in Figure 3, whereby $\delta O_2/N_2$ increases with both accumulation rate and temperature. This can be attributed to co-linearity between accumulation rate and temperature. We also note the non-linear response of density and grain size to perturbations in all forcings – most evident is the sensitivity of grain size to accumulation rate. This is in line with the dependence of $\delta O_2/N_2$ to the logarithm of accumulation rate documented in Figure 3.

3.2.4 Depth variability sensitivity

An alternative (although possibly complimentary) explanation for the mechanistic control of snow properties on elemental fractionation links to stratigraphic layering due to seasonality (Fujita et al., 2009). Here we explore the influence of layering by looking at the depth variability in density and grain size as a qualitative measure of stratification (Hörhold et al., 2011),

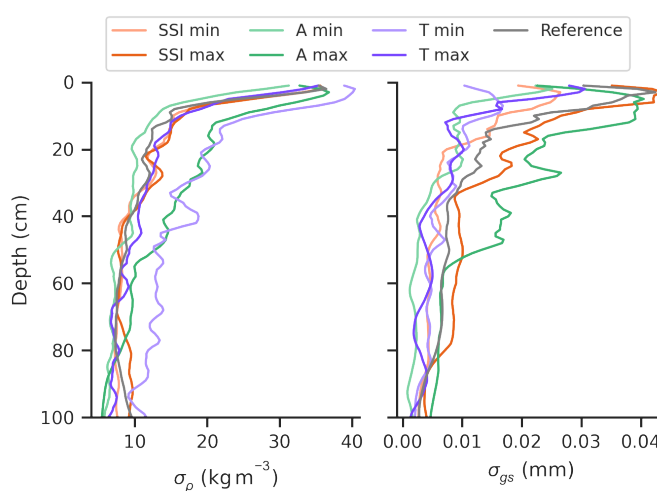


Figure 7. Variability in density and grain size with depth over the top 1 m. Each pair of simulations is represented by a colour, SSI in orange, accumulation rate in green, and temperature in purple. The faded line of each pair represents the 800-ka minimum simulation, and the bold line represents the 800-ka maximum simulation.



assuming that higher variability indicates stronger layering. Variability is defined as the standard deviation of each depth interval (denoted σ) over the period between January 1st 2010 and December 1st 2020.

The σ values for each simulation are presented in Figure 7 for the top 1 m of snowpack. In all runs, σ peaks near the surface and decreases with depth for both density and grain size (σ_ρ and σ_{gs}). Density variability for four out of the six test simulations is largely similar to the reference. High-accumulation rate (A max) and low-temperature (T min) are the exception, with an increase in σ_ρ of up to 5 kg m^{-3} compared to all other runs. Surprisingly, the increased σ_ρ values correspond to a decrease in mean density in the A max and T min simulations (Figure 6). The spread in σ_{gs} between simulations is broader than for σ_ρ over the top 50 cm, with T min, SSI min, A min, and T max all resulting in reduced variability compared to the reference run. σ_{gs} appears to increase with SSI and accumulation rate throughout the top metre.

To summarise, outputs from the Crocus model indicate that insolation modifies mean grain size but has negligible effect on mean density in the top 20 cm. On the other hand, higher air temperature and lower accumulation rate result in increases in both mean density and mean grain size, although this change is not necessarily proportional. The depth variability of the two snowpack parameters is strongly influenced by increased accumulation rate, with decreased temperature also having a large effect on density variability, and increased SSI causing an increase in grain size variability. At 100 cm, there is no significant difference in the σ_ρ and σ_{gs} for the different forcing scenarios, which is discussed in Section 4.3.2.

4 Discussion

4.1 Evidence for non-SSI dependence of $\delta\text{O}_2/\text{N}_2$

Our compilation of different deep ice core $\delta\text{O}_2/\text{N}_2$ records show the widely documented anti-correlation between SSI and $\delta\text{O}_2/\text{N}_2$ on the ice-age scale (Kawamura et al., 2007; Landais et al., 2012; Suwa and Bender, 2008a; Oyabu et al., 2021; Extier et al., 2018; Bouchet et al., 2023). However, a comparison of EDC, Dome F, and South Pole (as the only 3 cores with sufficient long and high resolution $\delta\text{O}_2/\text{N}_2$ records not affected by gas loss for this study) reveals an additional latitudinal dependence of the slope of the linear regression, whereby the highest latitudes have the steepest slope (SP $90^\circ\text{S} = -0.09\% \text{c.m}^2 \cdot \text{W}^{-1}$, DF $79^\circ\text{S} = -0.06\% \text{c.m}^2 \cdot \text{W}^{-1}$, EDC $75^\circ\text{S} = -0.05\% \text{c.m}^2 \cdot \text{W}^{-1}$; Figure 2). This suggests an additional influence of site conditions such as integrated summer insolation (ISI) (Huybers and Denton, 2008), which is not surprising given the mechanistic overlap with total air content (TAC) variability (Fujita et al., 2009). Inter-site analysis reveals a dependence of mean $\delta\text{O}_2/\text{N}_2$ on SSI (average over the last 1000 years) with both temporal (Figure 2) and spatial (Figure 3c) data falling on the same regression slope (mean $-0.07\% \text{c.m}^2 \cdot \text{W}^{-1}$). We also observe new evidence that mean $\delta\text{O}_2/\text{N}_2$ is significantly dependent on local temperature and accumulation rate, most apparent in the dependence of mean $\delta\text{O}_2/\text{N}_2$ on the natural log of accumulation rate (Figure 3b).

Further investigation into drivers of $\delta\text{O}_2/\text{N}_2$ variability at Dome C revealed a significant dependence on δD (a proxy for accumulation rate and temperature on the long-time scale considered here). Between 190 and 260 ka BP at Dome C, the residuals of the $\delta\text{O}_2/\text{N}_2$ -SSI regression are strongly correlated with δD ($r=0.62$, $p<0.001$), both on the AICC2012 ice-age scale. This relationship is maintained in four out of five sections of high-resolution measurements from the EDC core (Figure S3), with the age-range of the outlying section (409–449 ka BP) coinciding with onset of MIS 11 (424–374 ka BP).



The temporal analysis from Dome C initially contradicts the findings from Kobashi et al. (2015), who show an anti-
415 correlation between accumulation rate and $\delta\text{Ar}/\text{N}_2$ (and thus, $\delta\text{O}_2/\text{N}_2$) at GISP2, Greenland. However, this anti-correlation
is observed when $\delta\text{Ar}/\text{N}_2$ is drawn on a gas-age scale while our observations are performed on $\delta\text{O}_2/\text{N}_2$ drawn on the ice-age
scale. Moreover, (Suwa and Bender, 2008b) found a positive correlation between millennial-scale $\delta\text{O}_2/\text{N}_2$ variability and local
temperature at GISP2. This apparent contrast in the link between $\delta\text{O}_2/\text{N}_2$ (or $\delta\text{Ar}/\text{N}_2$) and accumulation rate variability
is also reflected in TAC records. Superimposed to orbital variations driven by ISI (Lipenkov et al., 2011), TAC also exhibits
420 shorter, millennial-scale variations which are correlated with accumulation rate at SP, Antarctica (Epifanio et al., 2023) but
anti-correlated at NGRIP, Greenland (Eicher et al., 2016) – all considered on the gas-age scale. The observations from Kobashi
et al. (2015) and Eicher et al. (2016) suggest additional mechanisms may be at play at high accumulation sites in Greenland,
which are evident in the $\delta\text{O}_2/\text{N}_2$ and TAC records over millennial timescales. Our overarching aim is to improve the use of
 $\delta\text{O}_2/\text{N}_2$ as a dating tool, and therefore, we focus on the mechanisms controlling $\delta\text{O}_2/\text{N}_2$ variability at Antarctica sites - or
425 rather, low accumulation sites - where accumulation increase leads to an increase in $\delta\text{O}_2/\text{N}_2$.

4.2 Proposed mechanisms controlling $\delta\text{O}_2/\text{N}_2$ variability

Several mechanisms have been proposed to explain variations in $\delta\text{O}_2/\text{N}_2$ and TAC and could be considered in light of our
new findings; namely, 1) the effect of residence time in the LIZ, specifically referring to the time taken for pores to close-off
(Severinghaus and Battle, 2006; Lipenkov et al., 2011), 2) transient effects from rapid climatic changes driving variations in
430 overburden pressure on the closing bubbles (Kobashi et al., 2015; Eicher et al., 2016), and 3) effects of near-surface snow
properties and layering which persist throughout the firm (Bender, 2002; Fujita et al., 2009; Severinghaus and Battle, 2006;
Gregory et al., 2014).

1) Severinghaus and Battle (2006) stated that at low accumulation sites, pores will close-off deeper and take longer to fully
close, thus, experiencing more total gas loss and, presumably, more elemental fractionation. Moreover, low accumulation sites
435 are usually characterised by a thin lock-in zone which facilitates diffusivity and fugitive gas loss, as is evidenced by young
gas ages in deep firm open porosity (Landais, 2004; Witrant et al., 2012). It is plausible that this ‘residence time’ effect could
partially explain our observations of a positive correlation between accumulation rate and $\delta\text{O}_2/\text{N}_2$. However, we would expect
this signal to be imprinted on the gas-age scale – or more likely, an integrated signal over the entire firm column – and as such,
this effect alone cannot account for the much stronger correlation between accumulation rate/temperature and $\delta\text{O}_2/\text{N}_2$ on the
440 ice-age scale at Dome C.

2) Short-term (millennial-scale) variations of $\delta\text{O}_2/\text{N}_2$ ($\delta\text{Ar}/\text{N}_2$) and TAC with accumulation rate have been linked to transient
effects in the firm column, resulting from rapid climatic changes (Kobashi et al., 2015; Eicher et al., 2016). During the initial
stage of a Dansgaard-Oeschger event, rapid increases in accumulation rate cause overburden pressure to increase, while more
time is needed for the firm column temperature to respond (Eicher et al., 2016). Eicher et al. (2016) suggest that these transient
445 effects explain the anti-correlation observed between accumulation rate and TAC on the gas-age scale at high-accumulation
sites. On the other hand, Kobashi et al. (2015) propose an alternative microbubble mechanism to explain the $\delta\text{Ar}/\text{N}_2$ response to
rapid climatic change. Such effects are expected to be negligible at low-accumulation sites such as Dome C where accumulation



variations are gradual. Moreover, the associated direction of change in $\delta O_2/N_2$ during high accumulation conditions is opposite to our observations, potentially indicating that the dominant mechanisms vary between low- and high-accumulation sites, as suggested by Epifanio et al. (2023) with regard to TAC.

3) Near-surface snow properties and layer stratification have been invoked to modulate $\delta O_2/N_2$ variability since the first study of Bender (2002). The signal of near surface snow metamorphism - imprinted in the grain properties - is generally understood to persist throughout the densification process to the close-off depth, influencing pore closure processes (Bender, 2002). Kawamura et al. (2007) also suggested a link between the strength of metamorphism at the surface and the existence of the lock-in zone leading to $\delta O_2/N_2$ fractionation. In parallel, Raynaud et al. (2007) proposed that the metamorphism induced by stronger insolation accelerates grain growth at the surface which later controls porosity in the lock in zone. Fujita et al. (2009) were the first to focus explicitly on the physical mechanisms governing both elemental fractionation during pore closure and total air content. They provided microstructural data – such as grain size, anisotropy, and a qualitative measure of permeability – from a Dome Fuji firn core and suggested a link between SSI and deep firn density stratification and permeability. They proposed that gas transport via permeation would be more efficient when there is a strong density stratification; such that, increased SSI leads to bulk ice with lower $\delta O_2/N_2$ - which agrees with what we observe. However, these studies do not explicitly explore the link between local climate (accumulation rate and temperature) and $\delta O_2/N_2$ variability.

4.3 Towards a mechanistic understanding of $\delta O_2/N_2$ variability at low-accumulation sites

While a link between climate and snow metamorphism has been evidenced in previous studies - whereby snow metamorphism is enhanced during summers with very low accumulation rates (Picard et al., 2012; Casado et al., 2021) – the link to pore closure processes has received less attention. Our analysis aims to bridge this gap by focusing on both local climate parameters and SSI, their influence on near-surface snow metamorphism, and how this might modulate elemental fractionation during pore closure. Crocus snowpack sensitivity tests were used in this study as a first step towards understanding a mechanistic link between physical properties and $\delta O_2/N_2$ variability. Our findings support a density-dependent grain size mechanism linking snow metamorphism and elemental fractionation at close-off. Indeed, Calonne et al. (2022) showed that grain size has a strong influence on permeability, such that for a given density, permeability is increased with grain size. Moreover, Gregory et al. (2014) found that permeability is increased in high-density, large-grain size firn due to a less complex pore structure. The following sections utilise the qualitative differences in bulk snow properties and stratification obtained from the Crocus sensitivity tests to develop a mechanistic explanation for the role of snow properties on pore closure fractionation.

4.3.1 The role of bulk snow properties

SSI sensitivity tests (S min and S max in Table 2) show an increase in grain size under increased SSI, attributed to both increases in near-surface temperature gradients (Appendix B in Vionnet et al., 2012) and increased snow temperature (Figure S4 in supplement) during summer. The absence of a density response to perturbations in SSI forcing is unclear. In reality, negligible change, or even a decrease, in near-surface density may be attributed to mass loss via sublimation (Inoue et al.,



480 2023). However, vapour transport is not modelled in Crocus and it is therefore more likely that this artifact is linked to the compaction scheme.

The sensitivity of bulk grain size to accumulation rate can be linked to the indirect effect of the residence time of a snow layer in the upper centimetres of the snowpack, where temperature gradients are strongest (Vionnet et al., 2012; Picard et al., 2012). Shorter residence time with increased accumulation rate (A max) impedes snow metamorphism, resulting in smaller
485 grain size, and vice versa. A corresponding decrease in snow density under A max facilitates grain growth (Eq. B1 in Vionnet et al., 2012), but this effect is minor compared to the residence time. Increased grain size in T max can be attributed to an increase in the rate of snow metamorphism with temperature, independent of changes in temperature gradient (Legagneux et al., 2003).

Based on the results presented in our study, the anti-correlation between SSI and $\delta O_2/N_2$ is coherent with an increase in
490 near-surface grain size for a given density, leading to bulk ice with decreased $\delta O_2/N_2$. The opposite – a decrease in grain size for a given density – would thus result in bulk ice with increased $\delta O_2/N_2$. Under this rationale, our results suggest a dominant influence of accumulation rate over temperature, given the decreased grain size under A max conditions. We note, however, that accumulation rate and temperature co-vary and thus this interpretation is oversimplified. Regardless, a stronger correlation between $\delta O_2/N_2$ and accumulation rate than temperature in Figure 3 supports the dominant role of accumulation rate at low
495 accumulation sites. However, increased grain growth with temperature (Figure 6) contradicts this interpretation, highlighting a sensitive balance between temperature driven snow metamorphism, and accumulation driven burial rates. Our findings suggest a link between bulk ice $\delta O_2/N_2$ and density-dependent grain size near the surface, but also suggest the importance of snow/firn residence time, both near the surface, and in the LIZ.

4.3.2 The role of depth-dependent variability as a proxy for layering

500 The role of SSI and local climate on deep firn layering is considered by determining the sensitivity of density and grain size variability near the surface. Making the link between variability near the surface and variability in deep firn is not straightforward. Indeed, a study by Hörhold et al. (2011) used a compilation of firn cores from numerous polar sites to show that density variability in deep firn is positively correlated with local accumulation rate and temperature, but anti-correlated with near-surface density variability. Although, this anti-correlation was not observed by Inoue et al. (2023) when comparing firn
505 cores in the Dome Fuji area where the range of accumulation rate (temperature) was narrower. Additional consideration is required for density inversions in the firn column - whereby low-density layers located in the upper part of the firn become high-density layers below the density inversion depth, due to preferential deformation in the upper firn (Freitag et al., 2004; Fujita et al., 2009). Moreover, stratification at depth may also be influenced by impurity content, with impurity rich layers being more susceptible to densification (Hörhold et al., 2012).

510 Increased grain size variability in SSI max in Figure 7 supports the conclusions of Fujita et al. (2009) that layering is enhanced with SSI due to increased seasonality in snow temperature and temperature gradients, and vice versa. Conversely, decreased grain size variability in both the increased and decreased temperature simulations is likely linked to the way in which temperature forcing is perturbed. By applying a constant increase in air temperature, the strength of metamorphism is increased



during winter due to higher temperatures (Legagneux et al., 2003; Flanner and Zender, 2006), while snow temperatures during
515 summer are less effected (Figure S4) – due to the dominant influence of insolation on summer snow temperature. The weaker
effect during summer results in homogeneity in the snowpack. Opposingly, a decrease in temperature would suppress meta-
morphism throughout the year – as evidenced by a decrease in mean grain size (Figure 6) - resulting in relatively decreased
variability in the snowpack. The combined influence of accumulation rate and temperature perturbations is expected to result in
a complex response in both σ_ρ and σ_{gs} . Moreover, the variability – and bulk mean – differences are likely to be very sensitive to
520 the ascribed glacial and interglacial accumulation rate and temperature values, leading to potentially inaccurate interpretations.
This is particularly important for glacial temperature reconstructions which are debated to have been overestimated by up to
5°C (Buizert, 2021).

Extracting concrete conclusions from the variability analysis and extrapolating these into the deep firn is inhibited by both
the ascribed forcing perturbations and the aggregation scheme of the model, which is particularly sensitive to changes in
525 accumulation rate. We thus conclude that the simulations performed with the Crocus model can support a mechanism of bulk
grain size on $\delta O_2/N_2$ in ice but not a mechanism implying grain size variability. However, our conclusion does not rule out the
effect of layering or grain size variability on $\delta O_2/N_2$ variability but highlights a limitation in our study, as explained in the next
section.

4.4 Perspectives and limitations

530 As noted in Section 3.2.1, there is a cold bias in simulated surface temperature compared to observations during summer, which
is expected to be consistent between simulations. We therefore argue that this should not influence our qualitative interpretations
of the anomalies in density and grain size (relative to the reference), especially considering that Crocus accurately reproduces
density and grain size profiles (Figure 5). The variability, however, is not fully captured by the model and can be explained
by the absence of snow transport by the wind in the standard version of Crocus (Libois et al., 2014). Libois et al. (2014) were
535 able to improve the variability reproducibility in the top 50cm using a multi-patch approach to account for snow transport
by the wind. Further, Inoue et al. (2023) found that wind speed was the major factor controlling density variability from 6
cores near Dome Fuji. While the effects of wind on snow properties are important (Pinzer and Schneebeli, 2009; Dacic et al.,
2015; Inoue et al., 2023), the absence of wind transport from our simulations is not expected to influence the results from the
sensitivity tests. Moreover, from a paleo-climatological perspective, we are limited in our understanding of winds throughout
540 the Quaternary. In parallel, the aggregation of layers with depth in Crocus make it difficult to focus on both the fine-layered
near-surface snow, and the propagation of stratified layers into the deep firn. Accurate assessment of the layering effect would
require a new dedicated snow model preserving individual snow layers and properties over a large depth range, from the surface
to LIZ, and at high resolution.

We also reiterate that accumulation rate depends on temperature which in turn is linked to local SSI. We maintain that
545 the single-parameter sensitivity tests presented here provide useful insights for understanding physical mechanisms, but do
not account for complex compound effects expected in reality. Indeed, additional tests perturbing multiple forcing parameters
simultaneously indicate that snowpack properties are very sensitive to the ascribed accumulation rate and temperature values.

Because this modelling approach also has weaknesses, as detailed above, we did not use it for interpretation of compound effects in this study.

550 A number of commonly proposed mechanisms to explain $\delta\text{O}_2/\text{N}_2$ variability were considered in our analysis. However, it is important to note that there are other possible explanatory mechanisms. The influence of microstructural properties beyond grain size has not been discussed but poses an alternative mechanistic explanation for elemental fractionation during pore closure. Hutterli et al. (2009) theoretically showed that changes in near surface temperature gradients under varying climate states modulate the anisotropy of the ice due to variations in temperature gradient metamorphism. This theory was recently
555 confirmed by Leinss et al. (2020) who found that snow anisotropy was predominantly driven by vertical water vapour fluxes in the near-surface snow. Periods of high SSI facilitate temperature gradient metamorphism in the vertical, resulting in elongated pores allowing more fractionation (Hutterli et al., 2009; Leinss et al., 2020). Similarly, low accumulation rates will prolong the residence time of snow layers near the surface where temperature gradients are strongest, thus facilitating snow metamorphism (e.g. Inoue et al., 2023). While assessing pore shape and anisotropy is outside the scope of this study, the direction of change is
560 consistent with our results, such that periods of high accumulation rate, and temperature, would reduce near-surface temperature gradient metamorphism, allowing less fractionation resulting in increased $\delta\text{O}_2/\text{N}_2$.

We lastly consider the bias towards low accumulation sites in our study. The majority of the datasets included in this study were relatively low-resolution, which limited the analysis of non-orbital temporal variability. While peaks in $\delta\text{O}_2/\text{N}_2$ corresponding to Dansgaard-Oeschger events are apparent in data from GISP2, which was previously observed by (Suwa and
565 Bender, 2008b), much of the data was either of too low resolution or influenced by storage gas-loss to perform additional analysis. The limited availability and temporal range of $\delta\text{O}_2/\text{N}_2$ records from Greenland cores meant that our study is slightly biased towards Antarctic sites, which tend to be characterised by low accumulation rates. Given this bias, we were unable to explore the opposing millennial-scale behaviour observed at low and high accumulation sites for both $\delta\text{O}_2/\text{N}_2$ and TAC (Kobashi et al., 2015; Eicher et al., 2016). Future studies would therefore benefit from obtaining high resolution measurements
570 from sites with different characteristics.

5 Conclusions

We present a compilation of $\delta\text{O}_2/\text{N}_2$ records measured on multiple ice cores from Greenland and Antarctica, to improve the mechanistic explanation for $\delta\text{O}_2/\text{N}_2$ variability. Analysis of both spatial (multi-site) and temporal (single-site) variability in $\delta\text{O}_2/\text{N}_2$ revealed new evidence of a dependence on local climate (accumulation rate and temperature), in addition to the
575 well-documented insolation dependence. High resolution measurements from the EDC ice core hinted to a millennial-scale variability in $\delta\text{O}_2/\text{N}_2$ behaving in-phase with δD records when both parameters are plotted on the AICC2012 ice-age scale. The inter-site analysis revealed an increase in mean $\delta\text{O}_2/\text{N}_2$ for sites with higher accumulation rate and temperature, which is analogous with the temporal analysis from EDC showing $\delta\text{O}_2/\text{N}_2$ to increase together with δD .

We argue for a dominant firm physical properties mechanism which links both the influence of SSI and local climate to
580 $\delta\text{O}_2/\text{N}_2$ variability on the ice-age scale by modulating near-surface snow properties. Sensitivity tests using the Crocus model



show that grain size is very responsive to perturbations in SSI, accumulation rate and air temperature, while density responds to all but SSI perturbations. Our findings support a grain size mechanism partially controls elemental fractionation during pore closure, such that increased grain size for a given density facilitates O₂ expulsion via enhanced permeability. We argue that the presence, or lack thereof at sites such as Dome Fuji (Kawamura et al., 2007), of a local climatic signal in $\delta\text{O}_2/\text{N}_2$ variability
585 is due to the delicate balance between the counter-effects of accumulation rate and temperature on grain properties. However, the inter-site results suggest that low accumulation, low temperature sites experience stronger elemental fractionation, having a comparable effect to high insolation.

While our findings from the $\delta\text{O}_2/\text{N}_2$ data compilation can be supported by the Crocus sensitivity tests, we acknowledge that there may be more complex mechanisms at play. In particular, the influence of deep firn layering – itself linked to surface snow
590 metamorphism – could not be tested fully in this study but is believed to play a major role on bulk ice $\delta\text{O}_2/\text{N}_2$. Determining the relative influence of stratification, firn physical properties and residence time in the lock-in zone, using firn models would be useful for future studies.

Code availability. The Crocus model is open-source, and the code is available at https://opensource.umr-cnrm.fr/projects/snowtools_git/wiki/Procedure_for_new_users. The version used is labeled as Surfex V8_1.

595 *Data availability.* All unpublished $\delta\text{O}_2/\text{N}_2$ data measured at LSCE will be made available online. Published datasets are available online at the references in Table S2 in the supplement.

Author contributions. AL, EC and FP performed measurements/produced the unpublished datasets measured at LSCE - on ice provided by RM and BS - and CB and JS provided unpublished datasets measured at Scripps. Snow temperature data from Dome C was acquired and shared by LA and GP. RHS ran the Crocus simulations, with the support of MD and QL. RHS and AL prepared the manuscript with
600 contributions from all co-authors.

Competing interests. At least one of the authors is a member of the editorial board of The Cryosphere.

Acknowledgements. This publication was generated in the frame of DEEPICE project. The project has received funding from the European Union's Horizon 2020 research and innovation programme under the Marie Skłodowska-Curie grant agreement No 955750. The measurements leading to these results has also received funding from the European Union's H2020 Programme (H2020/20192024)/ERC
605 grant agreement no. 817493 (ERC ICORDA). EC acknowledges the financial support from the French National Research Agency under the "Programme d'Investissements d'Avenir" (ANR-19-MPGA-0001). MD has received funding from the European Research Council (ERC)



under the European Union's Horizon 2020 research and innovation program (IVORI; grant no. 949516). We also thank Matthieu Fructus for providing his expertise and support in the Crocus model.

Financial support. This research has been supported by the Horizon 2020 research and innovation programme (grant no. 955750 and grant
610 no. 817493).



References

- Albert, M., Shuman, C., Courville, Z., Bauer, R., Fahnestock, M., and Scambos, T.: Extreme firn metamorphism: impact of decades of vapor transport on near-surface firn at a low-accumulation glazed site on the East Antarctic plateau, *Annals of Glaciology*, 39, 73–78, <https://doi.org/10.3189/172756404781814041>, 2004.
- 615 Alley, R. B. and Koci, B. R.: Ice-core analysis at site A, Greenland: preliminary results, *Annals of Glaciology*, 10, 1–4, <https://doi.org/10.3189/S0260305500004067>, 1988.
- Alley, R. B., Meese, D., Shuman, C., Gow, A., Taylor, K., Grootes, P., White, J., Ram, M., Waddington, E., Mayewski, P., et al.: Abrupt increase in Greenland snow accumulation at the end of the Younger Dryas event, *Nature*, 362, 527–529, <https://doi.org/10.1038/362527a0>, 1993.
- 620 Arnaud, L., Barnola, J. M., and Duval, P.: Physical modeling of the densification of snow/ firn and ice in the upper part of polar ice sheets, in: *Physics of ice core records*, pp. 285–305, Hokkaido University Press, <http://hdl.handle.net/2115/32472>, 2000.
- Battle, M., Bender, M., Sowers, T., Tans, P., Butler, J., Elkins, J., Ellis, J., Conway, T., Zhang, N., Lang, P., et al.: Atmospheric gas concentrations over the past century measured in air from firn at the South Pole, *Nature*, 383, 231–235, <https://doi.org/10.1038/383231a0>, 1996.
- 625 Bazin, L., Landais, A., Lemieux-Dudon, B., Toyé Mahamadou Kele, H., Veres, D., Parrenin, F., Martinerie, P., Ritz, C., Capron, E., Lipenkov, V., Loutre, M.-F., Raynaud, D., Vinther, B., Svensson, A., Rasmussen, S. O., Severi, M., Blunier, T., Leuenberger, M., Fischer, H., Masson-Delmotte, V., Chappellaz, J., and Wolff, E.: An optimized multi-proxy, multi-site Antarctic ice and gas orbital chronology (AICC2012): 120dash;800 ka, *Climate of the Past*, 9, 1715–1731, <https://doi.org/10.5194/cp-9-1715-2013>, 2013.
- Bazin, L., Landais, A., Capron, E., Masson-Delmotte, V., Ritz, C., Picard, G., Jouzel, J., Dumont, M., Leuenberger, M., and Prié, F.:
630 Phase relationships between orbital forcing and the composition of air trapped in Antarctic ice cores, *Climate of the Past*, 12, 729–748, <https://doi.org/10.5194/cp-12-729-2016>, 2016.
- Bender, M., Sowers, T., and Lipenkov, V.: On the concentrations of O₂, N₂, and Ar in trapped gases from ice cores, *Journal of Geophysical Research: Atmospheres*, 100, 18 651–18 660, <https://doi.org/10.1029/94JD02212>, 1995.
- Bender, M. L.: Orbital tuning chronology for the Vostok climate record supported by trapped gas composition, *Earth and Planetary Science Letters*, 204, 275–289, [https://doi.org/https://doi.org/10.1016/S0012-821X\(02\)00980-9](https://doi.org/https://doi.org/10.1016/S0012-821X(02)00980-9), 2002.
- 635 Bender, M. L., Tans, P. P., Ellis, J., Orchardo, J., and Habfast, K.: A high precision isotope ratio mass spectrometry method for measuring the O₂N₂ ratio of air, *Geochimica et Cosmochimica Acta*, 58, 4751–4758, [https://doi.org/https://doi.org/10.1016/0016-7037\(94\)90205-4](https://doi.org/https://doi.org/10.1016/0016-7037(94)90205-4), 1994.
- Bertler, N. A., Conway, H., Dahl-Jensen, D., Emanuelsson, U., Winstrup, M., Vallelonga, P. T., Lee, J. E., Brook, E. J., Severinghaus, J. P.,
640 Fudge, T. J., Keller, E. D., Baisden, W. T., Hindmarsh, R. C. A., Neff, P. D., Blunier, T., Edwards, R. L., Mayewski, P. A., Kipfstuhl, S., Buizert, C., Canessa, S., Dacic, R., Kjær, H. A., Kurbatov, A., Zhang, D., Waddington, E. D., Baccolo, G., Beers, T., Brightley, H. J., Carter, L., Clemens-Sewall, D., Ciobanu, V. G., Delmonte, B., Eling, L., Ellis, A. A., Ganesh, S., Golledge, N. R., Haines, S. A., Handley, M., Hawley, R. L., Hogan, C. M., Johnson, K. M., Korotkikh, E., Lowry, D. P., Mandeno, D., McKay, R. M., Menking, J. A., Naish, T. R., Noerling, C., Ollive, A., Orsi, A. J., Proemse, B. C., Pyne, A. R., Pyne, R. L., Renwick, J., Scherer, R. P., Semper, S., Simonsen, M., Sneed, S. B., Steig, E. J., Tuohy, A., Ulayottil Venugopal, A., Valero Delgado, F., Venkatesh, J., Wang, F., Wang, S., Winski, D. A.,
645 Winton, V. H. L., Whiteford, A., Xiao, C., Yang, J., and Zhang, X.: Roosevelt Island Climate Evolution (RICE) ice core isotope record, <https://doi.org/10.1594/PANGAEA.880396>, 2017.



- Bertler, N. A. N., Conway, H., Dahl-Jensen, D., Emanuelsson, D. B., Winstrup, M., Vallelonga, P. T., Lee, J. E., Brook, E. J., Severinghaus, J. P., Fudge, T. J., Keller, E. D., Baisden, W. T., Hindmarsh, R. C. A., Neff, P. D., Blunier, T., Edwards, R.,
650 Mayewski, P. A., Kipfstuhl, S., Buizert, C., Canessa, S., Dacic, R., Kjær, H. A., Kurbatov, A., Zhang, D., Waddington, E. D., Bac-
colo, G., Beers, T., Brightley, H. J., Carter, L., Clemens-Sewall, D., Ciobanu, V. G., Delmonte, B., Eling, L., Ellis, A., Ganesh,
S., Golledge, N. R., Haines, S., Handley, M., Hawley, R. L., Hogan, C. M., Johnson, K. M., Korotkikh, E., Lowry, D. P.,
Mandeno, D., McKay, R. M., Menking, J. A., Naish, T. R., Noerling, C., Ollive, A., Orsi, A., Proemse, B. C., Pyne, A. R.,
Pyne, R. L., Renwick, J., Scherer, R. P., Semper, S., Simonsen, M., Sneed, S. B., Steig, E. J., Tuohy, A., Venugopal, A. U.,
655 Valero-Delgado, F., Venkatesh, J., Wang, F., Wang, S., Winski, D. A., Winton, V. H. L., Whiteford, A., Xiao, C., Yang, J., and
Zhang, X.: The Ross Sea Dipole – temperature, snow accumulation and sea ice variability in the Ross Sea region, Antarctica,
over the past 2700 years, *Climate of the Past*, 14, 193–214, <https://doi.org/10.5194/cp-14-193-2018>, 2018.
- Bouchet, M., Landais, A., Grisart, A., Parrenin, F., Prié, F., Jacob, R., Fourré, E., Capron, E., Raynaud, D., Lipenkov, V. Y., Loutre, M.-F.,
Extier, T., Svensson, A., Legrain, E., Martinerie, P., Leuenberger, M., Jiang, W., Ritterbusch, F., Lu, Z.-T., and Yang, G.-M.: The Antarctic
660 Ice Core Chronology 2023 (AICC2023) chronological framework and associated timescale for the European Project for Ice Coring in
Antarctica (EPICA) Dome C ice core, *Climate of the Past*, 19, 2257–2286, <https://doi.org/10.5194/cp-19-2257-2023>, 2023.
- Buiron, D., Chappellaz, J., Stenni, B., Frezzotti, M., Baumgartner, M., Capron, E., Landais, A., Lemieux-Dudon, B., Masson-Delmotte,
V., Montagnat, M., et al.: TALDICE-1 age scale of the Talos Dome deep ice core, East Antarctica, *Climate of the Past*, 7, 1–16,
<https://doi.org/10.5194/cp-7-1-2011>, 2011.
- 665 Buizert, C.: The Ice Core Gas Age-Ice Age Difference as a Proxy for Surface Temperature, *Geophysical Research Letters*, 48,
e2021GL094241, <https://doi.org/10.1029/2021GL094241>, 2021.
- Buizert, C., Martinerie, P., Petrenko, V., Severinghaus, J., Trudinger, C., Witrant, E., Rosen, J., Orsi, A., Rubino, M., Etheridge, D., et al.: Gas
transport in firn: multiple-tracer characterisation and model intercomparison for NEEM, Northern Greenland, *Atmospheric Chemistry and
Physics*, 12, 4259–4277, <https://doi.org/10.5194/acp-12-4259-2012>, 2012.
- 670 Buizert, C., Baggenstos, D., Bereiter, B., Bertler, N., Brook, E. J., and Etheridge, D.: Multi-site ice core Krypton stable isotope ratios,
<https://doi.org/10.15784/601394>, 2020.
- Buizert, C., Shackleton, S., Severinghaus, J. P., Roberts, W. H. G., Seltzer, A., Bereiter, B., Kawamura, K., Baggenstos, D., Orsi, A. J.,
Oyabu, I., Birner, B., Morgan, J. D., Brook, E. J., Etheridge, D. M., Thornton, D., Bertler, N., Pyne, R. L., Mulvaney, R., Mosley-
Thompson, E., Neff, P. D., and Petrenko, V. V.: The new Kr-86 excess ice core proxy for synoptic activity: West Antarctic storminess
675 possibly linked to Intertropical Convergence Zone (ITCZ) movement through the last deglaciation, *Climate of the Past*, 19, 579–606,
<https://doi.org/10.5194/cp-19-579-2023>, 2023.
- Calonne, N., Burr, A., Philip, A., Flin, F., and Geindreau, C.: Effective coefficient of diffusion and permeability of firn at Dome C and
Lock In, Antarctica, and of various snow types – estimates over the 100–850 kg m⁻³ density range, *The Cryosphere*, 16, 967–980,
<https://doi.org/10.5194/tc-16-967-2022>, 2022.
- 680 Capron, E., Landais, A., Chappellaz, J., Schilt, A., Buiron, D., Dahl-Jensen, D., Johnsen, S. J., Jouzel, J., Lemieux-Dudon, B., Loulergue,
L., Leuenberger, M., Masson-Delmotte, V., Meyer, H., Oerter, H., and Stenni, B.: Millennial and sub-millennial scale climatic variations
recorded in polar ice cores over the last glacial period, *Climate of the Past*, 6, 345–365, <https://doi.org/10.5194/cp-6-345-2010>, 2010.
- Capron, E., Landais, A., Buiron, D., Cauquoin, A., Chappellaz, J., Debret, M., Jouzel, J., Leuenberger, M., Martinerie, P., Masson-Delmotte,
V., Mulvaney, R., Parrenin, F., and Prié, F.: Glacial–interglacial dynamics of Antarctic firn columns: comparison between simulations and
685 ice core air-delta;¹⁵N measurements, *Climate of the Past*, 9, 983–999, <https://doi.org/10.5194/cp-9-983-2013>, 2013.



- Carmagnola, C., Morin, S., Lafaysse, M., Domine, F., Lesaffre, B., Lejeune, Y., Picard, G., and Arnaud, L.: Implementation and evaluation of prognostic representations of the optical diameter of snow in the SURFEX/ISBA-Crocus detailed snowpack model, *The Cryosphere*, 8, 417–437, <https://doi.org/10.5194/tc-8-417-2014>, 2014.
- Casado, M., Landais, A., Picard, G., Arnaud, L., Dreossi, G., Stenni, B., and Prié, F.: Water Isotopic Signature of Surface Snow Metamorphism in Antarctica, *Geophysical Research Letters*, 48, e2021GL093382, <https://doi.org/https://doi.org/10.1029/2021GL093382>, 2021.
- 690 Champollion, N., Picard, G., Arnaud, L., Lefebvre, E., Macelloni, G., Rémy, F., and Fily, M.: Marked decrease in the near-surface snow density retrieved by AMSR-E satellite at Dome C, Antarctica, between 2002 and 2011, *The Cryosphere*, 13, 1215–1232, <https://doi.org/10.5194/tc-13-1215-2019>, 2019.
- Clow, G. D.: GISP2-D Temperature, <https://doi.org/10.1594/PANGAEA.55517>, 1999.
- 695 Crotti, I., Landais, A., Stenni, B., Bazin, L., Parrenin, F., Frezzotti, M., Ritterbusch, F., Lu, Z.-T., Jiang, W., Yang, G.-M., et al.: An extension of the TALDICE ice core age scale reaching back to MIS 10.1, *Quaternary Science Reviews*, 266, 107078, <https://doi.org/10.1016/j.quascirev.2021.107078>, 2021.
- Cuffey, K. M. and Clow, G. D.: GISP2 accumulation rate history, <https://doi.org/10.1594/PANGAEA.56075>, 1999.
- Dadic, R., Schneebeli, M., Bertler, N. A., Schwikowski, M., and Matzl, M.: Extreme snow metamorphism in the Allan Hills, Antarctica, as an analogue for glacial conditions with implications for stable isotope composition, *Journal of Glaciology*, 61, 1171–1182, <https://doi.org/10.3189/2015JoG15J027>, 2015.
- 700 Domine, F., Salvatori, R., Legagneux, L., Salzano, R., Fily, M., and Casacchia, R.: Correlation between the specific surface area and the short wave infrared (SWIR) reflectance of snow, *Cold Regions Science and Technology*, 46, 60–68, <https://doi.org/https://doi.org/10.1016/j.coldregions.2006.06.002>, 2006.
- 705 Eicher, O., Baumgartner, M., Schilt, A., Schmitt, J., Schwander, J., Stocker, T. F., and Fischer, H.: Climatic and insolation control on the high-resolution total air content in the NGRIP ice core, *Climate of the Past*, 12, 1979–1993, <https://doi.org/10.5194/cp-12-1979-2016>, 2016.
- EPICA community members: One-to-one coupling of glacial climate variability in Greenland and Antarctica, *Nature*, 444, 195–198, <https://doi.org/10.1038/nature05301>, 2006.
- 710 Epifanio, J. A., Brook, E. J., Buizert, C., Pettit, E. C., Edwards, J. S., Fegyveresi, J. M., Sowers, T. A., Severinghaus, J. P., and Kahle, E. C.: Millennial and orbital-scale variability in a 54 000-year record of total air content from the South Pole ice core, *The Cryosphere*, 17, 4837–4851, <https://doi.org/10.5194/tc-17-4837-2023>, 2023.
- Etheridge, D. and Wookey, C.: Ice core drilling at a high accumulation area of Law Dome, Antarctica, 1987, in: *Ice Core Drilling, Proceedings of the Third International Workshop on Ice Core Drilling Technology*, Grenoble, France, pp. 86–96, 1988.
- 715 Extier, T., Landais, A., Bréant, C., Prié, F., Bazin, L., Dreyfus, G., Roche, D. M., and Leuenberger, M.: On the use of $\delta^{18}\text{O}_{\text{atm}}$ for ice core dating, *Quaternary Science Reviews*, 185, 244–257, <https://doi.org/https://doi.org/10.1016/j.quascirev.2018.02.008>, 2018.
- Fegyveresi, J. M., Alley, R., Spencer, M., Fitzpatrick, J., Steig, E., White, J., McConnell, J., and Taylor, K.: Late-Holocene climate evolution at the WAIS Divide site, West Antarctica: bubble number-density estimates, *Journal of Glaciology*, 57, 629–638, <https://doi.org/10.3189/002214311797409677>, 2011.
- 720 Flanner, M. G. and Zender, C. S.: Linking snowpack microphysics and albedo evolution, *Journal of Geophysical Research: Atmospheres*, 111, <https://doi.org/https://doi.org/10.1029/2005JD006834>, 2006.
- Freitag, J., Wilhelms, F., and Kipfstuhl, S.: Microstructure-dependent densification of polar firn derived from X-ray microtomography, *Journal of Glaciology*, 50, 243–250, <https://doi.org/10.3189/172756504781830123>, 2004.



- 725 Frezzotti, M., Pouchet, M., Flora, O., Gandolfi, S., Gay, M., Urbini, S., Vincent, C., Becagli, S., Gragnani, R., Proposito, M., et al.: New estimations of precipitation and surface sublimation in East Antarctica from snow accumulation measurements, *Climate Dynamics*, 23, 803–813, <https://doi.org/10.1007/s00382-004-0462-5>, 2004.
- Fudge, T. J., Buizert, C., Conway, H., and Waddington, E. D.: Accumulation Rates from the WAIS Divide Ice Core, <https://doi.org/110.15784/601004>, 2017.
- Fujita, S., Kawada, K., and Fujii, Y.: Glaciological Data Collected by the 37th Japanese Antarctic Research Expedition during 1996-1997, 730 JARE data reports, 27, 1–46, <https://doi.org/10.15094/00004965>, 1998.
- Fujita, S., Okuyama, J., Hori, A., and Hondoh, T.: Metamorphism of stratified firn at Dome Fuji, Antarctica: A mechanism for local insolation modulation of gas transport conditions during bubble close off, *Journal of Geophysical Research: Earth Surface*, 114, <https://doi.org/https://doi.org/10.1029/2008JF001143>, 2009.
- Gallet, J.-C., Domine, F., and Dumont, M.: Measuring the specific surface area of wet snow using 1310 nm reflectance, *The Cryosphere*, 8, 735 1139–1148, <https://doi.org/10.5194/tc-8-1139-2014>, 2014.
- Gkinis, V., Vinther, B. M., Popp, T. J., Quistgaard, T., Faber, A.-K., Holme, C. T., Jensen, C.-M., Lanzky, M., Lütt, A.-M., Mandrakis, V., et al.: A 120,000-year long climate record from a NW-Greenland deep ice core at ultra-high resolution, *Scientific data*, 8, 141, <https://doi.org/10.1038/s41597-021-00916-9>, 2021.
- Gregory, S. A., Albert, M. R., and Baker, I.: Impact of physical properties and accumulation rate on pore close-off in layered firn, *The Cryosphere*, 8, 91–105, <https://doi.org/10.5194/tc-8-91-2014>, 2014.
- Grenfell, T. C., Warren, S. G., and Mullen, P. C.: Reflection of solar radiation by the Antarctic snow surface at ultraviolet, visible, and near-infrared wavelengths, *Journal of Geophysical Research: Atmospheres*, 99, 18 669–18 684, <https://doi.org/10.1029/94JD01484>, 1994.
- Hamilton, G. S.: Mass balance and accumulation rate across Siple Dome, West Antarctica, *Annals of Glaciology*, 35, 102–106, <https://doi.org/10.3189/172756402781816609>, 2002.
- 745 Hersbach, H., Bell, B., Berrisford, P., Hirahara, S., Horányi, A., Muñoz-Sabater, J., Nicolas, J., Peubey, C., Radu, R., Schepers, D., et al.: The ERA5 global reanalysis, *Quarterly Journal of the Royal Meteorological Society*, 146, 1999–2049, <https://doi.org/10.1002/qj.3803>, 2020.
- Hoffmann, H. M., Grieman, M. M., King, A. C., Epifanio, J. A., Martin, K., Vladimirova, D., Pryer, H. V., Doyle, E., Schmidt, A., Humby, J. D., et al.: The ST22 chronology for the Skytrain Ice Rise ice core–Part 1: A stratigraphic chronology of the last 2000 years, *Climate of the Past*, 18, 1831–1847, <https://doi.org/10.5194/cp-18-1831-2022>, 2022.
- 750 Hörhold, M., Kipfstuhl, S., Wilhelms, F., Freitag, J., and Frenzel, A.: The densification of layered polar firn, *Journal of Geophysical Research: Earth Surface*, 116, <https://doi.org/10.1029/2009JF001630>, 2011.
- Hörhold, M., Laepple, T., Freitag, J., Bigler, M., Fischer, H., and Kipfstuhl, S.: On the impact of impurities on the densification of polar firn, *Earth and Planetary Science Letters*, 325, 93–99, <https://doi.org/https://doi.org/10.1016/j.epsl.2011.12.022>, 2012.
- Huber, C., Beyerle, U., Leuenberger, M., Schwander, J., Kipfer, R., Spahni, R., Severinghaus, J., and Weiler, K.: Evidence for molecular size dependent gas fractionation in firn air derived from noble gases, oxygen, and nitrogen measurements, *Earth and Planetary Science Letters*, 755 243, 61–73, <https://doi.org/https://doi.org/10.1016/j.epsl.2005.12.036>, 2006.
- Hutterli, M. A., Schneebeli, M., Freitag, J., Kipfstuhl, J., and Röthlisberger, R.: Impact of local insolation on snow metamorphism and ice core records, *Physics of Ice Core Records II*, 68, 223–232, <http://hdl.handle.net/2115/45450>, 2009.
- Huybers, P. and Denton, G.: Antarctic temperature at orbital timescales controlled by local summer duration, *Nature Geoscience*, 1, 787–792, 760 <https://doi.org/10.1038/ngeo311>, 2008.



- Ikeda-Fukazawa, T., Fukumizu, K., Kawamura, K., Aoki, S., Nakazawa, T., and Hondoh, T.: Effects of molecular diffusion on trapped gas composition in polar ice cores, *Earth and Planetary Science Letters*, 229, 183–192, <https://doi.org/https://doi.org/10.1016/j.epsl.2004.11.011>, 2005.
- Inoue, R., Fujita, S., Kawamura, K., Oyabu, I., Nakazawa, F., and Motoyama, H.: Evolution of layered density and microstructure in near-surface firn around Dome Fuji, Antarctica, *EGUsphere*, 2023, 1–43, <https://doi.org/10.5194/egusphere-2023-1838>, 2023.
- 765 Jouzel, J., Masson-Delmotte, V., Cattani, O., Dreyfus, G., Falourd, S., Hoffmann, G., Minster, B., Nouet, J., Barnola, J.-M., Chappellaz, J., et al.: Orbital and millennial Antarctic climate variability over the past 800,000 years, *science*, 317, 793–796, <https://doi.org/10.1126/science.1141038>, 2007.
- Kahle, E., Buizert, C., Conway, H., Epifanio, J., Fudge, T. J., and Jones, T. R.: Temperature, accumulation rate, and layer thinning from the South Pole ice core (SPC14), <https://doi.org/10.15784/601396>, 2020.
- 770 Kawamura, K., Parrenin, F., Lisiecki, L., Uemura, R., Vimeux, F., Severinghaus, J. P., Hutterli, M. A., Nakazawa, T., Aoki, S., Jouzel, J., et al.: Northern Hemisphere forcing of climatic cycles in Antarctica over the past 360,000 years, *Nature*, 448, 912–916, <https://doi.org/10.1038/nature06015>, 2007.
- Kobashi, T., Ikeda-Fukazawa, T., Suwa, M., Schwander, J., Kameda, T., Lundin, J., Hori, A., Motoyama, H., Döring, M., and Leuenberger, M.: Post-bubble close-off fractionation of gases in polar firn and ice cores: effects of accumulation rate on permeation through overloading pressure, *Atmospheric Chemistry and Physics*, 15, 13 895–13 914, <https://doi.org/10.5194/acp-15-13895-2015>, 2015.
- 775 Landais, A.: Rapid climate variability in the North Atlantic: the contribution of air isotopes trapped in Greenland ice, Phd thesis, Laboratoire des Sciences du Climat et de l'Environnement [Gif-sur-Yvette], Paris, FR, available at <https://www.theses.fr/2004PA066185>, 2004.
- Landais, A., Chappellaz, J., Delmotte, M., Jouzel, J., Blunier, T., Bourg, C., Caillon, N., Cherrier, S., Malaizé, B., Masson-Delmotte, V., Raynaud, D., Schwander, J., and Steffensen, J. P.: A tentative reconstruction of the last interglacial and glacial inception in Greenland based on new gas measurements in the Greenland Ice Core Project (GRIP) ice core, *Journal of Geophysical Research: Atmospheres*, 108, <https://doi.org/https://doi.org/10.1029/2002JD003147>, 2003.
- 780 Landais, A., Dreyfus, G., Capron, E., Pol, K., Loutre, M. F., Raynaud, D., Lipenkov, V. Y., Arnaud, L., Masson-Delmotte, V., Paillard, D., Jouzel, J., and Leuenberger, M.: Towards orbital dating of the EPICA Dome C ice core using $\delta^{18}\text{O}_2/\text{N}_2$, *Climate of the Past*, 8, 191–203, <https://doi.org/10.5194/cp-8-191-2012>, 2012.
- 785 Laskar, J., Robutel, P., Joutel, F., Gastineau, M., Correia, A. C. M., and Levrard, B.: A long-term numerical solution for the insolation quantities of the Earth, *AA*, 428, 261–285, <https://doi.org/10.1051/0004-6361:20041335>, 2004.
- Lazzara, M. A., Keller, L. M., Markle, T., and Gallagher, J.: Fifty-year Amundsen–Scott South Pole station surface climatology, *Atmospheric Research*, 118, 240–259, <https://doi.org/https://doi.org/10.1016/j.atmosres.2012.06.027>, 2012.
- 790 Lee, J. E., Brook, E. J., Bertler, N. A. N., Buizert, C., Baisden, T., Blunier, T., Ciobanu, V. G., Conway, H., Dahl-Jensen, D., Fudge, T. J., Hindmarsh, R., Keller, E. D., Parrenin, F., Severinghaus, J. P., Vallelonga, P., Waddington, E. D., and Winstrup, M.: An 83 000-year-old ice core from Roosevelt Island, Ross Sea, Antarctica, *Climate of the Past*, 16, 1691–1713, <https://doi.org/10.5194/cp-16-1691-2020>, 2020.
- Legagneux, L., Cabanes, A., and Dominé, F.: Measurement of the specific surface area of 176 snow samples using methane adsorption at 77 K, *Journal of Geophysical Research: Atmospheres*, 107, ACH–5, <https://doi.org/10.1029/2001JD001016>, 2002.
- 795 Legagneux, L., Lauzier, T., Dominé, F., Kuhs, W. F., Heinrichs, T., and Techmer, K.: Rate of decay of specific surface area of snow during isothermal experiments and morphological changes studied by scanning electron microscopy, *Canadian Journal of Physics*, 81, 459–468, <https://doi.org/10.1139/p03-025>, 2003.



- Leinss, S., Löwe, H., Proksch, M., and Kontu, A.: Modeling the evolution of the structural anisotropy of snow, *The Cryosphere*, 14, 51–75, <https://doi.org/10.5194/tc-14-51-2020>, 2020.
- 800 Libois, Q., Picard, G., France, J. L., Arnaud, L., Dumont, M., Carmagnola, C. M., and King, M. D.: Influence of grain shape on light penetration in snow, *The Cryosphere*, 7, 1803–1818, <https://doi.org/10.5194/tc-7-1803-2013>, 2013.
- Libois, Q., Picard, G., Arnaud, L., Morin, S., and Brun, E.: Modeling the impact of snow drift on the decameter-scale variability of snow properties on the Antarctic Plateau, *Journal of Geophysical Research: Atmospheres*, 119, 11,662–11,681, <https://doi.org/https://doi.org/10.1002/2014JD022361>, 2014.
- 805 Libois, Q., Picard, G., Arnaud, L., Dumont, M., Lafaysse, M., Morin, S., and Lefebvre, E.: Summertime evolution of snow specific surface area close to the surface on the Antarctic Plateau, *The Cryosphere*, 9, 2383–2398, <https://doi.org/10.5194/tc-9-2383-2015>, 2015.
- Lipenkov, V., Raynaud, D., Loutre, M., and Duval, P.: On the potential of coupling air content and O₂/N₂ from trapped air for establishing an ice core chronology tuned on local insolation, *Quaternary Science Reviews*, 30, 3280–3289, <https://doi.org/https://doi.org/10.1016/j.quascirev.2011.07.013>, 2011.
- 810 Lüthi, D., Bereiter, B., Stauffer, B., Winkler, R., Schwander, J., Kindler, P., Leuenberger, M., Kipfstuhl, S., Capron, E., Landais, A., Fischer, H., and Stocker, T. F.: CO₂ and O₂/N₂ variations in and just below the bubble–clathrate transformation zone of Antarctic ice cores, *Earth and Planetary Science Letters*, 297, 226–233, <https://doi.org/https://doi.org/10.1016/j.epsl.2010.06.023>, 2010.
- Martin, K. C., Buizert, C., Edwards, J. S., Kalk, M. L., Riddell-Young, B., Brook, E. J., Beaudette, R., Severinghaus, J. P., and Sowers, T. A.: Bipolar impact and phasing of Heinrich-type climate variability, *Nature*, pp. 1–5, <https://doi.org/10.1038/s41586-023-05875-2>, 2023.
- 815 Martinerie, P., Lipenkov, V. Y., Raynaud, D., Chappellaz, J., Barkov, N. I., , and Lorius, C.: Air content paleo record in the Vostok ice core (Antarctica): A mixed record of climatic and glaciological parameters, *Journal of Geophysical Research: Atmospheres*, 99, 10 565–10 576, <https://doi.org/https://doi.org/10.1029/93JD03223>, 1994.
- Matsuoka, K., Skoglund, A., and Roth, G.: *Quantarctica*, <https://doi.org/10.21334/npolar.2018.8516e961>, 2018.
- McDowell, I. E., Albert, M. R., Lieblappen, S. A., and Keegan, K. M.: Local Weather Conditions Create Structural Differences between
820 Shallow Firn Columns at Summit, Greenland and WAIS Divide, Antarctica, *Atmosphere*, 11, 1370, 2020.
- Members, N. C.: Eemian interglacial reconstructed from a Greenland folded ice core, *Nature*, 493, 489–494, <https://doi.org/10.1038/nature11789>, 2013.
- Mitchell, L. E., Buizert, C., Brook, E. J., Breton, D. J., Fegyveresi, J., Baggenstos, D., Orsi, A., Severinghaus, J., Alley, R. B., Albert, M., Rhodes, R. H., McConnell, J. R., Sigl, M., Maselli, O., Gregory, S., and Ahn, J.: Observing and model-
825 ing the influence of layering on bubble trapping in polar firn, *Journal of Geophysical Research: Atmospheres*, 120, 2558–2574, <https://doi.org/https://doi.org/10.1002/2014JD022766>, 2015.
- Moon, T. A., Fisher, M., Stafford, T., and Thurber, A.: *QGreenland (v3)*, 2023.
- Morgan, V., Wookey, C., Li, J., van Ommen, T., Skinner, W., and Fitzpatrick, : Site information and initial results from deep ice drilling on Law Dome, Antarctica, *Journal of Glaciology*, 43, 3–10, <https://doi.org/10.3189/S0022143000002768>, 1997.
- 830 Mosley-Thompson, E., Paskievitch, J. F., Gow, A. J., and Thompson, L. G.: Late 20th century increase in South Pole snow accumulation, *Journal of Geophysical Research: Atmospheres*, 104, 3877–3886, <https://doi.org/10.1029/1998JD200092>, 1999.
- Mulvaney, R., Alemany, O., and Possenti, P.: The Berkner Island (Antarctica) ice-core drilling project, *Annals of Glaciology*, 47, 115–124, <https://doi.org/10.3189/172756407786857758>, 2007.
- Mulvaney, R., Triest, J., and Alemany, O.: The James Ross Island and the Fletcher Promontory ice-core drilling projects, *Annals of Glaciol-
835 ogy*, 55, 179–188, <https://doi.org/10.3189/2014AoG68A044>, 2014.



- Mulvaney, R., Rix, J., Polfrey, S., Grieman, M., Martín, C., Nehrbass-Ahles, C., Rowell, I., Tuckwell, R., and Wolff, E.: Ice drilling on Skytrain Ice Rise and Sherman Island, Antarctica, *Annals of Glaciology*, 62, 311–323, <https://doi.org/10.1017/aog.2021.7>, 2021.
- Mulvaney, R., Wolff, E. W., Grieman, M. M., Hoffmann, H. H., Humby, J. D., Nehrbass-Ahles, C., Rhodes, R. H., Rowell, I. F., Parrenin, F., Schmidely, L., et al.: The ST22 chronology for the Skytrain Ice Rise ice core—Part 2: An age model to the last interglacial and disturbed deep stratigraphy, *Climate of the Past*, 19, 851–864, <https://doi.org/10.5194/cp-19-851-2023>, 2023.
- 840 Neff, P. D.: A review of the brittle ice zone in polar ice cores, *Annals of Glaciology*, 55, 72–82, <https://doi.org/10.3189/2014AoG68A023>, 2014.
- NGRIP project members: High-resolution record of Northern Hemisphere climate extending into the last interglacial period, *Nature*, 431, 147–151, <https://doi.org/10.1038/nature02805>, 2004.
- 845 Oerter, H., Wilhelms, F., Jung-Rothenhäusler, F., Göktas, F., Miller, H., Graf, W., and Sommer, S.: Accumulation rates in Dronning Maud Land, Antarctica, as revealed by dielectric-profiling measurements of shallow firn cores, *Annals of Glaciology*, 30, 27–34, <https://doi.org/10.3189/172756400781820705>, 2000.
- Oyabu, I., Kawamura, K., Uchida, T., Fujita, S., Kitamura, K., Hirabayashi, M., Aoki, S., Morimoto, S., Nakazawa, T., Severinghaus, J. P., and Morgan, J. D.: Fractionation of O₂/N₂ and Ar/N₂ in the Antarctic ice sheet during bubble formation and bubble-clathrate hydrate transition from precise gas measurements of the Dome Fuji ice core, *The Cryosphere*, 15, 5529–5555, <https://doi.org/10.5194/tc-15-5529-2021>, 2021.
- 850 Oyabu, I., Kawamura, K., Fujita, S., Inoue, R., Motoyama, H., Fukui, K., Hirabayashi, M., Hoshina, Y., Kurita, N., Nakazawa, F., Ohno, H., Sugiura, K., Suzuki, T., Tsutaki, S., Abe-Ouchi, A., Niwano, M., Parrenin, F., Saito, F., and Yoshimori, M.: Temporal variations of surface mass balance over the last 5000 years around Dome Fuji, Dronning Maud Land, East Antarctica, *Climate of the Past*, 19, 293–321, <https://doi.org/10.5194/cp-19-293-2023>, 2023.
- 855 Parrenin, F., Barnola, J.-M., Beer, J., Blunier, T., Castellano, E., Chappellaz, J., Dreyfus, G., Fischer, H., Fujita, S., Jouzel, J., et al.: The EDC3 chronology for the EPICA Dome C ice core, *Climate of the Past*, 3, 485–497, <https://doi.org/10.5194/cp-3-485-2007>, 2007.
- Petrenko, V. V., Severinghaus, J. P., Brook, E. J., Reeh, N., and Schaefer, H.: Gas records from the West Greenland ice margin covering the Last Glacial Termination: a horizontal ice core, *Quaternary Science Reviews*, 25, 865–875, <https://doi.org/https://doi.org/10.1016/j.quascirev.2005.09.005>, 2006.
- 860 Picard, G., Domine, F., Krinner, G., Arnaud, L., and Lefebvre, E.: Inhibition of the positive snow-albedo feedback by precipitation in interior Antarctica, *Nature Climate Change*, 2, 795–798, <https://doi.org/10.1038/nclimate1590>, 2012.
- Picard, G., Libois, Q., and Arnaud, L.: Refinement of the ice absorption spectrum in the visible using radiance profile measurements in Antarctic snow, *The Cryosphere*, 10, 2655–2672, <https://doi.org/10.5194/tc-10-2655-2016>, 2016.
- 865 Pinzer, B. R. and Schneebeli, M.: Snow metamorphism under alternating temperature gradients: Morphology and recrystallization in surface snow, *Geophysical research letters*, 36, <https://doi.org/10.1029/2009GL039618>, 2009.
- Rasmussen, S. O., Abbott, P. M., Blunier, T., Bourne, A., Brook, E., Buchardt, S. L., Buizert, C., Chappellaz, J., Clausen, H., Cook, E., et al.: A first chronology for the North Greenland Eemian Ice Drilling (NEEM) ice core, *Climate of the Past*, 9, 2713–2730, <https://doi.org/10.5194/cp-9-2713-2013>, 2013.
- 870 Raynaud, D., Lipenkov, V., Lemieux-Dudon, B., Duval, P., Loutre, M.-F., and Lhomme, N.: The local insolation signature of air content in Antarctic ice. A new step toward an absolute dating of ice records, *Earth and Planetary Science Letters*, 261, 337–349, <https://doi.org/https://doi.org/10.1016/j.epsl.2007.06.025>, 2007.



- Rubino, M., Etheridge, D., Trudinger, C., Allison, C., Battle, M., Langenfelds, R., Steele, L., Curran, M., Bender, M., White, J., et al.:
A revised 1000 year atmospheric $\delta^{13}\text{C}$ -CO₂ record from Law Dome and South Pole, Antarctica, *Journal of Geophysical Research:*
875 *Atmospheres*, 118, 8482–8499, <https://doi.org/10.1002/jgrd.50668>, 2013.
- Schwander, J., Sowers, T., Barnola, J.-M., Blunier, T., Fuchs, A., and Malaizé, B.: Age scale of the air in the summit ice:
Implication for glacial-interglacial temperature change, *Journal of Geophysical Research: Atmospheres*, 102, 19483–19493,
<https://doi.org/https://doi.org/10.1029/97JD01309>, 1997.
- Severinghaus, J.: Nitrogen and Oxygen Gas Isotopes in the Siple Dome and Byrd Ice Cores, Antarctica [Dataset],
880 <https://doi.org/10.7265/N55X26V0>, 2009.
- Severinghaus, J.: Low-res d¹⁵N and d¹⁸O of O₂ in the WAIS Divide 06A Deep Core [Dataset], <https://doi.org/10.7265/N5S46PWD>, 2015.
- Severinghaus, J.: South Pole (SPICECORE) 15N, 18O, O₂/N₂ and Ar/N₂ [Dataset], <https://doi.org/10.15784/601152>, 2019.
- Severinghaus, J. P. and Battle, M. O.: Fractionation of gases in polar ice during bubble close-off: New constraints from firm air Ne, Kr and
Xe observations, *Earth and Planetary Science Letters*, 244, 474–500, <https://doi.org/https://doi.org/10.1016/j.epsl.2006.01.032>, 2006.
- 885 Severinghaus, J. P., Grachev, A., and Battle, M.: Thermal fractionation of air in polar firm by seasonal temperature gradients, *Geochemistry,*
Geophysics, Geosystems, 2, <https://doi.org/10.1029/2000GC000146>, 2001.
- Shackleton, S. A.: Tracking Past Changes in Ocean Heat Content with Atmospheric Noble Gases in Ice Cores, Doctoral dissertation, Univer-
sity of California, San Diego, <http://dissertations.umi.com/ucsd:18809>, 2019.
- Sowers, T., Bender, M., and Raynaud, D.: Elemental and isotopic composition of occluded O₂ and N₂ in polar ice, *Journal of Geophysical*
890 *Research: Atmospheres*, 94, 5137–5150, <https://doi.org/https://doi.org/10.1029/JD094iD04p05137>, 1989.
- Stenni, B., Proposito, M., Gragnani, R., Flora, O., Jouzel, J., Falourd, S., and Frezzotti, M.: Eight centuries of volcanic sig-
nal and climate change at Talos Dome (East Antarctica), *Journal of Geophysical Research: Atmospheres*, 107, ACL–3,
<https://doi.org/10.1029/2000JD000317>, 2002.
- Stenni, B., Jouzel, J., Masson-Delmotte, V., Röthlisberger, R., Castellano, E., Cattani, O., Falourd, S., Johnsen, S., Longinelli, A., Sachs, J.,
895 et al.: A late-glacial high-resolution site and source temperature record derived from the EPICA Dome C isotope records (East Antarctica),
Earth and Planetary Science Letters, 217, 183–195, [https://doi.org/https://doi.org/10.1016/S0012-821X\(03\)00574-0](https://doi.org/https://doi.org/10.1016/S0012-821X(03)00574-0), 2004.
- Stenni, B., Masson-Delmotte, V., Selmo, E., Oerter, H., Meyer, H., Röthlisberger, R., Jouzel, J., Cattani, O., Falourd, S., Fischer, H., Hoff-
mann, G., Iacumin, P., Johnsen, S., Minster, B., and Udisti, R.: The deuterium excess records of EPICA Dome C and Dronning Maud Land
ice cores (East Antarctica), *Quaternary Science Reviews*, 29, 146–159, <https://doi.org/https://doi.org/10.1016/j.quascirev.2009.10.009>, cli-
900 mate of the Last Million Years: New Insights from EPICA and Other Records, 2010.
- Sturrock, G., Etheridge, D., Trudinger, C., Fraser, P., and Smith, A.: Atmospheric histories of halocarbons from analysis of Antarctic firm air:
Major Montreal Protocol species, *Journal of Geophysical Research: Atmospheres*, 107, ACH–12, <https://doi.org/10.1029/2002JD002548>,
2002.
- Suwa, M. and Bender, M. L.: Chronology of the Vostok ice core constrained by O₂/N₂ ratios of occluded air, and its implication for the Vostok
905 climate records, *Quaternary Science Reviews*, 27, 1093–1106, <https://doi.org/https://doi.org/10.1016/j.quascirev.2008.02.017>, 2008a.
- Suwa, M. and Bender, M. L.: O₂/N₂ ratios of occluded air in the GISP2 ice core, *Journal of Geophysical Research: Atmospheres*, 113,
<https://doi.org/https://doi.org/10.1029/2007JD009589>, 2008b.
- Tomoko Ikeda-Fukazawa, K. K. and Hondoh, T.: Mechanism of Molecular Diffusion in Ice Crystals, *Molecular Simulation*, 30, 973–979,
<https://doi.org/10.1080/08927020410001709307>, 2004.



- 910 Uemura, R., Motoyama, H., Masson-Delmotte, V., Jouzel, J., Kawamura, K., Goto-Azuma, K., Fujita, S., Kuramoto, T., Hirabayashi, M., Miyake, T., et al.: Asynchrony between Antarctic temperature and CO₂ associated with obliquity over the past 720,000 years, *Nature communications*, 9, 961, <https://doi.org/10.1038/s41467-018-03328-3>, 2018.
- Vionnet, V., Brun, E., Morin, S., Boone, A., Faroux, S., Le Moigne, P., Martin, E., and Willemet, J.-M.: The detailed snowpack scheme Crocus and its implementation in SURFEX v7.2, *Geoscientific Model Development*, 5, 773–791, <https://doi.org/10.5194/gmd-5-773-2012>, 2012.
- 915 Warren, S. G., Brandt, R. E., and Grenfell, T. C.: Visible and near-ultraviolet absorption spectrum of ice from transmission of solar radiation into snow, *Appl. Opt.*, 45, 5320–5334, <https://doi.org/10.1364/AO.45.005320>, 2006.
- Watanabe, O., Kamiyama, K., Motoyama, H., Fujii, Y., Shoji, H., , and Satow, K.: The paleoclimate recorded in the ice core from Dome Fuji station, Antarctica, *Journal of Geophysical Research: Atmospheres*, 29, 176—183, <https://doi.org/10.3189/172756499781821553>, 1999.
- White, J., Bradley, E., Garland, J., Jones, T. R., Morris, V., Price, M., and Vaughn, B.: table Isotopes of Ice in the Transition and Glacial
920 Sections of the WAIS Divide Deep Ice Core, <https://doi.org/10.15784/601274>, 2019.
- Winstrup, M., Vallenga, P., Kjær, H. A., Fudge, T. J., Lee, J. E., Riis, M. H., Edwards, R., Bertler, N. A. N., Blunier, T., Brook, E. J., Buizert, C., Ciobanu, G., Conway, H., Dahl-Jensen, D., Ellis, A., Emanuelsson, B. D., Hindmarsh, R. C. A., Keller, E. D., Kurbatov, A. V., Mayewski, P. A., Neff, P. D., Pyne, R. L., Simonsen, M. F., Svensson, A., Tuohy, A., Waddington, E. D., and Wheatley, S.: A 2700-year annual timescale and accumulation history for an ice core from Roosevelt Island, West Antarctica, *Climate of the Past*, 15, 751–779,
925 <https://doi.org/10.5194/cp-15-751-2019>, 2019.
- Wittrant, E., Martinerie, P., Hogan, C., Laube, J., Kawamura, K., Capron, E., Montzka, S., Dlugokencky, E., Etheridge, D., Blunier, T., et al.: A new multi-gas constrained model of trace gas non-homogeneous transport in firn: evaluation and behaviour at eleven polar sites, *Atmospheric Chemistry and Physics*, 12, 11 465–11 483, <https://doi.org/10.5194/acp-12-11465-2012>, 2012.